

Review article

Detection of hazardous volatile organic compounds (VOCs) by metal oxide nanostructures-based gas sensors: A review

A. Mirzaei ^a, S.G. Leonardi ^b, G. Neri ^{b,*}^a Department of Materials Engineering, Shiraz University, Shiraz, Iran^b Department of Engineering, University of Messina, Messina, Italy

ARTICLE INFO

Article history:

Received 9 May 2016

Received in revised form

21 June 2016

Accepted 22 June 2016

Available online 23 June 2016

Keywords:

Hazardous volatile organic compounds

VOCs

Gas sensors

Metal oxides

Nanostructures

ABSTRACT

Since the sensing capability of semiconducting metal oxides was demonstrated in the 1960s, solid state gas sensors based on these materials have attracted considerable attention from both scientific and practical point of view. Because of the promising characteristics for detecting toxic gases and volatile organic compounds (VOCs) compared to conventional techniques, these devices are expected to play a key role in environmental monitoring, chemical process control, personal safety and so on in the near future. Therefore, in recent years, intensive studies have been conducted to improve their sensing performances, particularly to increase the sensitivity and detection limit of such devices. This can be accomplished by using metal oxide nanostructures with various shapes such as nanoparticles, nanowires, nanorods and nanotubes having sizes in the nanometer range. Owing to the high surface-to-volume ratios and consequently large number of surface sites exposed to target gas, nanostructured metal oxides enable a larger gas-sensing layer interaction and hence a higher sensitivity in comparison with conventional materials.

This article extensively reviews recent developments in this field, focusing the attention on the detection of some common VOCs, including acetone (C_3H_6O), acetylene (C_2H_2), benzene (C_6H_6), cyclohexene (C_6H_{10}), ethanol (C_2H_5OH), formaldehyde ($HCHO$), n-butanol (C_4H_9OH), methanol (CH_3OH) toluene (C_7H_8), and 2-propanol (C_3H_8O), by means of conductometric solid state sensors based on nanostructured semiconducting metal oxides.

© 2016 Elsevier Ltd and Techna Group S.r.l. All rights reserved.

Contents

1. Introduction	15120
2. Volatile organic compounds: definition, types and general properties	15121
2.1. Acetone (C_3H_6O)	15121
2.2. Acetylene (C_2H_2)	15122
2.3. Benzene (C_6H_6)	15122
2.4. Cyclohexene (C_6H_{10})	15122
2.5. Ethanol (C_2H_5OH)	15122
2.6. Formaldehyde ($HCHO$)	15122
2.7. Methanol (CH_3OH)	15123
2.8. n-Butanol (C_4H_9OH)	15123
2.9. Toluene (C_7H_8)	15123
2.10. 2-propanol (C_3H_8O)	15123
3. Operating principle and detection mechanisms of semiconducting sensors	15123
4. Metal oxide nanostructures-based VOC sensors	15125
4.1. Ethanol sensors	15125
4.2. Acetone sensors	15128
4.3. Formaldehyde sensors	15129

* Corresponding author.

4.4. Toluene sensors	15131
4.5. Methanol sensors	15131
4.6. Acetylene sensors	15132
4.7. Benzene sensors	15134
4.8. Other VOC sensors	15134
5. Selectivity and effect of humidity	15135
6. Conclusions and outlook	15137
Acknowledgements	15138
References	15138

1. Introduction

Driving a car, cooking, making a fire, painting the house, cutting the grass, building materials, using pesticides or much simpler breathing, result in the emission of organic compounds such as carbonyls, alcohols, alkanes, alkenes, esters, aromatics, ethers, and amides. In other words, almost every human activity in daily life results in the release of organic species to the atmosphere [1]. Since the industrial revolution, many activities, such as the petroleum industry, have emitted anthropogenic pollutants including toxic gases and volatile organic compounds (VOCs) [2]. Some examples of specific sources and processes that commonly emit high levels of VOCs include vent gas, water separation techniques, industrial waste water, batch processes, petroleum refining, natural gas processing, petrochemical processes, and paints. Consequently, the increased emissions of VOCs and their resulting impact on the air quality are now considered as a major environmental concern.

Concentrations of VOCs are much higher indoors compared to outdoors (up to 10 times higher) and it is estimated that 50–300 different VOCs may be detected in the air of homes, schools, offices, and commercial buildings at any given time [3]. Also, a wide range of consumer and personal care products, during their use, can release significant amounts of VOCs into the air [4]. So, VOCs level is used as parameter to establish the air quality in indoor ambient, in addition to other indicators such as temperature and CO₂ levels [5].

Regarding the potential hazards of VOCs, a number of major environmental safety agencies, such as National Institute of Occupational Safety and Health (NIOSH), Environmental Protection Agency (EPA) and European Agency for Safety and Health at Work (EU-OSHA), have established guidelines to limit the exposure of humans to VOCs in indoor and workplace air because of their adverse effects on health, even at low (sub-ppb) concentrations [6].

Some volatile organic compounds have been identified as highly toxic or carcinogenic in nature and may have both short- and long-term impacts on human health as well as on the natural ecosystem. Benzene is a well-known example, which is a carcinogen with a high potential to damage humans both specifically (e.g., the liver, kidneys, spleen, and stomach) and systematically (e.g., the nervous, circulatory, reproductive, immune, cardiovascular, and respiratory systems). Another example is sick building syndrome (SBS), which is a health issue of significant importance and refers to situations where building occupants experience health issue, such as headaches, nausea, eye irritation, cough, etc., that develop from prolonged periods inside a building. Although no specific cause can be identified, factors associated with SBS include the temperature, odor, particulate matter and VOCs [7].

Therefore, effective methods to monitor VOCs have been in demand for atmospheric environmental measurement and control as well as human well-being and health monitoring. Accordingly, highly sensitive analytical techniques including spectrophotometry [8], gas chromatography (GC) [9] and high-

performance liquid chromatography (HPLC) [10] have been used for the accurate quantification of VOCs. Despite their accuracy and precision, these techniques generally have some drawbacks, such as great expense, lack of portability, high power demand, and low throughput. Moreover, the use of such techniques often requires complex and time consuming pre-treatment steps and highly skilled operators. The conventional method used for monitoring indoor VOCs is generally time-consuming and expensive because it involves on-site sampling of indoor air but ensuing the analysis of the sampled air in a laboratory. Clearly, these procedures cannot provide VOCs exposure information on a real-time basis. Therefore, inexpensive, small and user-friendly gas sensing devices are highly needed [11]. Up to date, considerable research and development have been conducted to design small, inexpensive and fast VOCs sensors with high sensitivity, selectivity and stability for specific applications [12]. This extensive research has led to a wide variety of VOCs sensors and devices based on different sensing principles, e.g. electrochemical, optical, gravimetric, resistive, etc. [6].

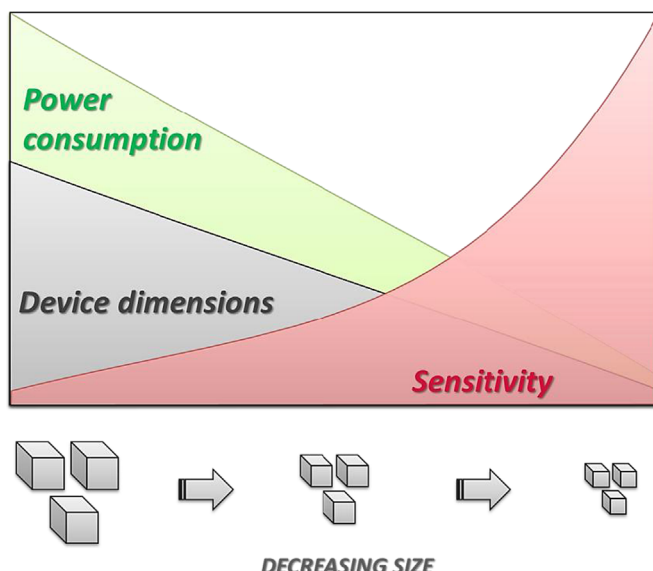
Table 1 presents the main types of sensors used for VOCs monitoring and their features. Up to date, no single sensor type demonstrates optimal performance overall, and which technology is most suited to a given application strongly depends on the operating requirements for that given application. Among the sensor devices considered, conductometric (resistive) gas sensors based on metal oxides are the most promising for monitoring harmful VOCs. The success of these types of devices are mainly due to their many advantages, such as strong response, high sensitivity, small dimensions, ease of use, portability, simple design, on-line operation, rapid response time, stable repeatability for reuse in the same process, simplicity in fabrication, compact size, real-time detection, low detection limits, low cost, and low power consumption [13–16]. On the other hand, despite the many worthy advantages, metal oxide sensors require high operating temperatures (typically 150–500 °C) and generally they have poor selectivity in detection of similar gaseous species [17].

In order to improve the performance of the metal oxide sensors, one of the most important approaches is the reduction of particle sizes to nanoscale in the sensing layer [22]. As the particles size is reduced, a higher specific surface area is obtained resulting in a large number of active sites which are beneficial for gas adsorption and consequently for a higher sensitivity. Furthermore, when the particles size of the sensing material is close to or less than double the thickness of a characteristic parameter known as “space-charge layer”, little changes of the charges due to the surface reactions with gas molecules will cause large changes of conductivity then a remarkably increase of the sensitivity occurs [23]. This type of advantage is expected with almost all the metal oxide nanostructures for gas sensing applications. Consequently, as shown in Fig. 1, the use of nanostructured materials could allow to reduce the geometrical area of sensitive element then decreasing the dimensions of the whole device while preserving high sensitivity [24]. Therefore, even if not directly, the use of

Table 1

Comparison of the working principle and different parameters of various gas sensors [18–21].

Sensor type	Resistive	Catalytic	Thermocapacitive	Electrochemical	Optical
Physical change/measured	Resistance	Temperature resistance	Temperature resistance voltage	Potential current	Transmission reflectance polarization phase shift
Parameters	Sensitivity	Excellent	Good	Bad	Good
	Selectivity	Poor	Bad	Bad	Good
	Stability	Good	Good	Good	Bad
	Response time	Excellent	Good	Good	Poor
	Accuracy	Good	Good	Good	Good
	Durability	Good	Good	Good	Poor
	Maintenance	Excellent	Excellent	Good	Good
	Portability	Excellent	Excellent	Good	Poor
	Cost	Cheap	Cheap	Cheap	Expensive
	Safety	Excellent	Risk of explosion	Good	Excellent
	Life time	Good	Excellent	Excellent	Good

**Fig. 1.** Possible positive effects of the use of nanosized materials as sensing elements on the sensors features.

nanomaterials in the manufacture of gas sensors, allowing to reduce the overall size of the devices and therefore the power needed to keep the sensors at their operating temperatures, it could result in an energy saving.

The above advantages have shifted the focus of the research community to synthesize sensing materials with the smallest particle size, while ensuring that their properties remain stable during the long term at high operational temperature, which is essential for practical sensors [25].

2. Volatile organic compounds: definition, types and general properties

In general, any chemical compound that contains at least one carbon and one hydrogen atom in its molecular structure is referred as an organic compound. Many hundreds of compounds come within the category of organic compounds and the situation is further complicated by the different definitions and nomenclature. Strictly speaking, the term, volatile organic compounds, (VOCs) refers to those organic compounds that are present in the atmosphere as gases, but would be liquids or solids under normal conditions of temperature and pressure.

According to the volatility, organic compounds can be classified into various categories, which include volatile organic compounds (VOCs), semi-volatile organic compounds (SVOCs) and non-volatile organic compounds (NVOCs). The term, VOC, in the United States is defined in the Code of Federal Regulations 40 CFR 51.100 (s) as follows: "VOC means any compound of carbon, excluding CO, CO₂, H₂CO₃, (NH₄)₂CO₃ and metallic carbides or carbonates, which participates in atmospheric photochemical reactions". The updated U.S. Environmental Protection Agency (EPA) definition is as follows: "VOCs are organic chemical compounds whose composition makes it possible for them to evaporate under normal indoor atmospheric conditions of temperature and pressure". The National Research Council described VOCs as "organic compounds that vaporize easily at room temperature". The European Union defined VOCs as any organic compound with an initial boiling point less than or equal to 250 °C measured at a standard pressure of 101.3 kPa. In Canada, the boiling points of VOCs were chosen roughly to be in the range of 50–250 °C. For volatile organic compounds such low boiling points means that they are easily vapors from liquid or solid surfaces into indoor or ambient air. Probably several thousand chemicals, both synthetic and natural, can be called VOCs [26].

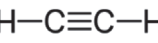
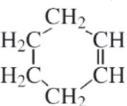
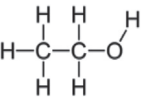
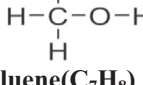
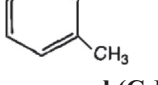
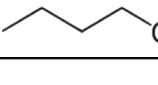
Table 2 lists the physical properties, IDLH (immediately dangerous to life or health) and TLV (threshold limit value) of VOCs. TLV is defined as the maximum concentration of a chemical permitted during a working day (8 h) for repeated exposure without producing adverse health effects [27]. In general VOCs are colorless, have very low boiling points, most of them are highly reactive and are often mixed with interfering gases [28].

2.1. Acetone (C_3H_6O)

It is a colorless liquid with a characteristic pungent odor, boiling point 56.5 °C, melting point –94 °C and density 0.788 gr/cm³ [29]. Acetone is a common reagent used widely in industries and laboratories. The compound is extensively used to dissolve plastics, purify paraffin and dehydrate tissues, and also is used in pharmaceuticals. Acetone is harmful to health and its inhalation can cause irritation of the eyes, nose, and throat. A short exposure for 5 min to 300–500 ppm can be slightly irritating to humans. In high concentrations, it can produce dryness in the mouth, fatigue, headache, nausea, dizziness, muscle weakness, loss of coordinated speech, and drowsiness. Ingestion can cause headache, dizziness, and dermatitis [29]. The inhalation of acetone causes headache, fatigue and even narcosis and harmfulness to nerve system. Therefore, it is necessary to monitor the acetone concentration in the environment for health and workplace for safety.

Table 2

Property and threshold limit values of VOCs in this review [29–31].

VOC name and formula	Properties	IDLH	TLV
Acetone (C₃H₆O) 	Colorless, pungent odor, sweetish taste, flammable	20,000 ppm NIOSH	750 ppm ACGIH
Acetylene (C₂H₂) 	Colorless, distinctive odor, low toxicity	N/A	N/A
Benzene(C₆H₆) 	Colorless, strong aroma, highly flammable, Chronic toxicity	500 ppm NIOSH	1 ppm OSHA
Cyclohexene (C₆H₁₀) 	Colorless, mild solvent odor, Flammable, low acute toxicity	10,000 ppm (NIOSH)	300 ppm ACGIH, OSHA, NIOSH
Ethanol (C₂H₅OH) 	Colorless, alcoholic smell and taste, flammable, low toxicity	3300 ppm NIOSH	1000 ppm OSHA
Formaldehyde (HCHO) 	Colorless, pungent odor, flammable, low acute toxicity	20 ppm NIOSH	0.75 ppm OSHA
Methanol (CH₃OH) 	Colorless, mild odor, flammable, high toxicity	25,000 ppm (NIOSH)	200 ppm (ACGIH)
Toluene(C₇H₈) 	Colorless, aromatic odor, highly flammable, slight acute toxicity	500 ppm NIOSH	100 ppm ACGIH, NIOSH, MSHA
2-propanol (C₃H₈O) 	Colorless, alcohol-like odor, bitter taste, Flammable low toxicity,	12,000 ppm NIOSH	400 ppm ACGIH
n-Butanol (C₄H₉OH) 	Colorless, vinous odor, flammable, slightly toxic	8000 ppm NIOSH	100 ppm NIOSH

2.2. Acetylene (C₂H₂)

It is a colorless, flammable unsaturated hydrocarbon gas with a distinctive odor. Since its boiling point at atmospheric pressure is 20.2 °C, it is an extremely volatile liquid. It is widely used as a fuel in oxyacetylene welding or cutting of metals and as a raw material in a range of industrial and consumer products, such as acet-aldehyde, synthetic rubber, paints, fabric and floor coverings, dry-cleaning solvents, and insecticide sprays. Acetylene is an extremely hazardous gas and notable hazards are associated with its intrinsic instability, particularly when it is liquefied, pressurized,

heated or mixed with air. Consequently, the combustion of acetylene can produce a large amount of heat (its highest flame temperature is approximately 3300 °C), and it can explode if the absolute pressure of the gas exceeds 103 kPa [32,33]. Therefore, for environmental and safety purposes, the development of a highly effective C₂H₂ sensor has become increasingly important to meet the demands of accurate environmental monitoring, for early leakage warning and to avoid incomplete combustion.

2.3. Benzene (C₆H₆)

It is a colorless liquid with a characteristic odor, density of 0.878 gr/cm³ at 20 °C and boiling point of 80.1 °C [29]. It is a by-product of many petrochemical processes, including oil refining. Until recently, benzene was used widely in industry as a solvent and a cleaning agent. In urban areas, it occurs in the exhaust fumes from motor vehicles and is a particular hazard in cities. The maximum permitted exposure limit in 2003 was set to 16.25 µg m⁻³ (or 5 ppb) [34]. Benzene is of particular concern because of its toxicity and carcinogenic properties. The narcotic effects in humans may occur from inhaling benzene in air at a concentration of 200 ppm. High concentrations can cause convulsions. A 5–10 min exposure to 2% benzene in air may be fatal. Death may result from respiratory failure. Benzene is a carcinogen via all routes of exposure and is known to be a major cause of leukemia and lymphomas [35].

2.4. Cyclohexene (C₆H₁₀)

It is a colorless liquid with boiling point 83 °C, melting point 103.5 °C and density 0.8098 gr/cm³ at 20 °C. It is used in making adipic acid, maleic acid, and butadiene, in oil extraction as a stabilizer for high-octane gasoline, and in organic synthesis. Inhalation produces irritation of the eyes and respiratory tract. It is also an irritant to skin. Its acute toxicity is low; the toxic effects are similar to those of cyclohexane. Exposure to high concentrations or ingestion may cause drowsiness [29].

2.5. Ethanol (C₂H₅OH)

Ethanol (C₂H₅OH) or ethyl alcohol is a colorless, clear, volatile liquid with sweetish smell and taste, boiling point of 78.3 °C, melting point of –114 °C; vapor pressure of 43 T at 20 °C and density of 0.789 gr/cm³ at 20 °C [29]. Ethanol, which is an inflammable chemical compound, is one of the most commonly and widely used alcohols and has many applications in food, biomedical, transportation, and chemical industries as well as health and safety [29,36]. Although the exposure to ethanol vapor is not dangerous, it could result in health problems such as headache, drowsiness, irritation of eyes and difficulty in breathing [37]. However, because of its extensive use as a beverage, one of the main causes of car accidents in the world is due to ethanol consumption, thus the quantitative detection of ethanol vapor at ppm levels is not only of medical, but also of social importance.

2.6. Formaldehyde (HCHO)

It is a colorless, flammable, widespread gas in air at room temperature. Therefore, people are mostly exposed to formaldehyde by inhalation. Low-level exposure to formaldehyde can cause damage to the human body, related symptoms, such as eye and throat irritations, chest tightness and shortness of breath [37]. As the smallest and most abundant aldehyde, it is one of the most important carbonyl compounds and one of the most important air pollutants in residential and industrial occupational environments. Although formaldehyde is toxic and allergenic, it is still used

widely in industrial processes owing to its high reactivity and relatively low cost. Formaldehyde is used mainly in the production of urea, phenolic and melamine resins [31]. The most common symptoms related to formaldehyde exposure include irritation to the eyes, nose and throat, which occurs at air concentrations of approximately 0.4–1 ppm (ppm). Higher concentrations (> 3 ppm) induce cytotoxic effects (cell and tissue damage). Moreover, formaldehyde has been classified as a human carcinogen because it causes nasopharyngeal cancer, pulmonary damage and probably leukemia at levels of 6 ppm [38]. Owing to the toxicity of formaldehyde, the World Health Organization (WHO) has established limits of exposure to formaldehyde to a maximum of 0.08 ppm averaged over 30 min. The OSHA has also set a permissible exposure limit for formaldehyde of 0.75 ppm for an 8 h workday [31].

2.7. Methanol (CH_3OH)

Methanol (CH_3OH) or methyl alcohol is a colorless liquid with a mild odor, boiling point of 65.15 °C melting point of –93.9 °C and a density of 0.7914 gr/cm³ at 20 °C. Methanol is a very useful organic solvent with widespread applications in automotive fuel and manufacturing of colors, dyes, drugs, perfumes, formaldehyde, etc. Methanol is highly toxic, causing acidosis and blindness. The symptoms of methanol poisoning include nausea, abdominal pain, headache, blurred vision, shortness of breath, and dizziness. Inhalation in humans may produce headache, drowsiness and eye irritation. Prolonged skin contact may cause dermatitis and scaling. Eye contact can cause burns and damage vision [29,39].

2.8. n-Butanol ($\text{C}_4\text{H}_9\text{OH}$)

n-Butanol ($\text{C}_4\text{H}_9\text{OH}$) or 1-butanol is a colorless liquid with a characteristic vinous odor, melting point –90 °C, boiling point 117.2 °C, and density 0.810 gr/cm³ at. This compound is used in the production of butyl acetate, butyl glycol ether and plasticizers, such as dibutyl phthalate, as a solvent in the coating industry, as a solvent for extractions of oils, drugs, and cosmetic nail products; and as an ingredient for perfumes and flavor. Exposing to n-butanol environment could cause symptoms such as dizziness, headache somnolence and dermatitis. In addition, it was found to cause severe injury to rabbits' eyes and to penetrate the cornea upon instillation into the eyes. Chronic exposure of humans to high concentrations may cause photophobia, blurred vision and lacrimation [29].

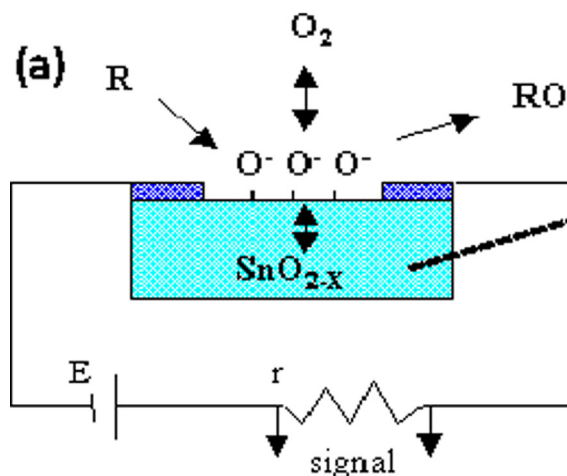


Fig. 2. a) Schematization of a resistive semiconductor gas sensor, b) Typical morphology of a metal oxide based sensing element.

2.9. Toluene (C_7H_8)

It is a colorless liquid with a characteristic aromatic odor; density of 0.866 gr/cm³ at 20 °C and boiling point of 110.7 °C [29]. Toluene is a benzenoid aromatic hydrocarbon that is emitted in the process of making gasoline and other fuels from crude oil and the making of coke from coal. This compound is used in the production of paints, paint thinners, fingernail polish, lacquers, adhesives, and rubber and in some printing and leather tanning processes [7]. The acute toxicity of toluene is similar to that of benzene, and the organs affected from its exposure are the central nervous system, liver, kidneys, and skin [29]. The WHO has set the guideline value for an indoor air concentration of 0.07 ppm for toluene at 25 °C. The 0.07 ppm toluene value (WHO) emphasizes the need for sensitive, specific, affordable, simple, and reproducible methods for detecting toluene gas [7].

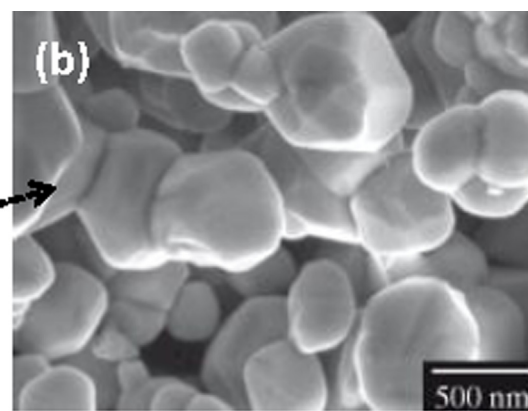
2.10. 2-propanol ($\text{C}_3\text{H}_8\text{O}$)

2-propanol ($\text{C}_3\text{H}_8\text{O}$) or isopropyl alcohol is a colorless liquid with an alcohol-like odor, bitter taste, boiling point of 82.3 °C and melting point of –89.5 °C, and a density of 0.7849 gr/cm³ at 20 °C. It is used in the production of acetone and isopropyl halides and is employed widely as an industrial solvent for paints, polishes and insecticides, as an antiseptic (rubbing alcohol), and in organic synthesis for introducing isopropyl or isopropoxy groups into molecules. Inhalation produces mild irritation to the eyes and nose. At 400–5500 ppm concentrations isopropanol causes a deterioration of the ciliary activity in guinea pigs. Ingestion causes drowsiness, dizziness and nausea. A large dose may result in coma [29].

3. Operating principle and detection mechanisms of semi-conducting sensors

Metal oxide semiconductor sensors are conductometric (resistive) type devices, therefore, the variation of electrical conductivity (resistivity) of the sensitive element is the variable related to the concentration of VOCs species. The basic structure of these sensors is simple. Fig. 2 shows the construction principle and the electrical readout circuit of a conductometric sensors based on non-stoichiometric tin dioxide (SnO_{2-x}). The typical morphology of the sensing element, showing the grain size of metal oxide, is also evidenced.

In metal oxides the resistance in air is due to the influence of surface reactions including electron exchange between



chemisorbed oxygen species and the metal oxide. Oxygen species from air ambient adsorb on the surface of semiconducting metal oxide particles in the ionic forms as $O_2^{(ads)}$, $O_{(ads)}^-$ and $O_{(ads)}^{2-}$. However, chemisorption is an energy activated processes and each oxygen species requires different temperature to take place on the grains surface. The $O_{(ads)}^{2-}$, requiring high activation energy to be chemisorbed, is normally presented at higher temperatures while the other ones are the probable ionic species at lower temperatures. In particular, at the temperatures lower than 400 °C, where most of metal oxide based VOCs sensors work, the $O_{(ads)}^-$ is the predominant species [40].

The gas sensing mechanism is essentially explained by the energy-band bending theory. When O_2 molecules are adsorbed on the surface of metal oxides, they would extract electrons from the conduction band by trapping charges at the grain surface in the form of ions. From a practical point of view, it is possible to assume that the delocalization of electrons from the bulk of the grains to their surface resulting in the formation of holes in the bulk and an accumulation of negative charge on the surface. This leads to the formation of an electron depleted region, called space-charge layer, then in an energy-band bending. Between grains the merging of the two depletion regions leads to an energetic interface known as Schottky barrier the magnitude of which depends on the conductivity of the material [41]. The reaction of adsorbed oxygen species with adsorbed VOCs can modify the intensity of Schottky barrier [42], resulting in a variation of conductivity (Fig. 3). Because the magnitude of energy level is directly related to the number of molecules reacting with the metal oxide surface, the variation of electrical parameter of the sensor (i.e. resistance, current) could be used as variable to monitor the concentration of VOCs species.

The sensitivity in changing the energy barrier when the metal oxides interact with the analyte species is strongly affected by the grains sizes. In particular, when the metal oxide structure is in the range of nanosize, the sensitivity is drastically enhanced. To better understand this effect it is possible to think the sensitive material as consisting of aggregate particles which are in contact with each other. As discussed earlier, when the oxygen adsorbs on the grains surface a space-charge layer of an appropriate width is formed. The difference in size between twice the width of the space-charge layer (L) and the grain size (d) leads to three distinctive cases (Fig. 4) [23]. When the grains sizes are sufficiently large ($d \gg 2L$),

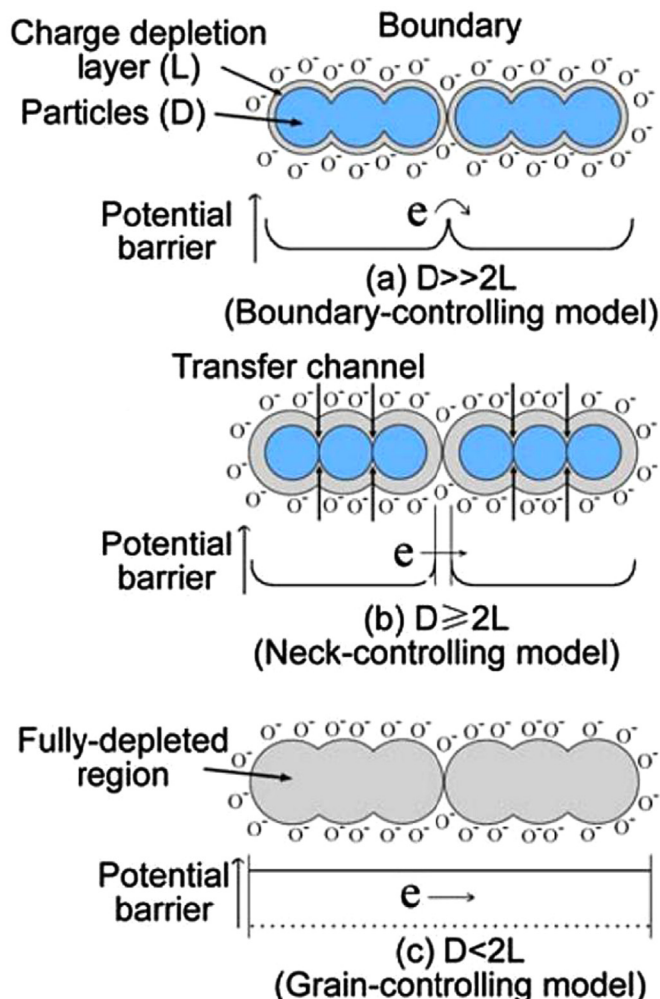


Fig. 4. Schematic model of the effect of the crystallite size on the sensitivity of metal-oxide gas sensors [23].

the conductivity of the material depends essentially on the mobility of the carriers inside the grains. Under these conditions, small variations of the potential barrier, result of surface effects

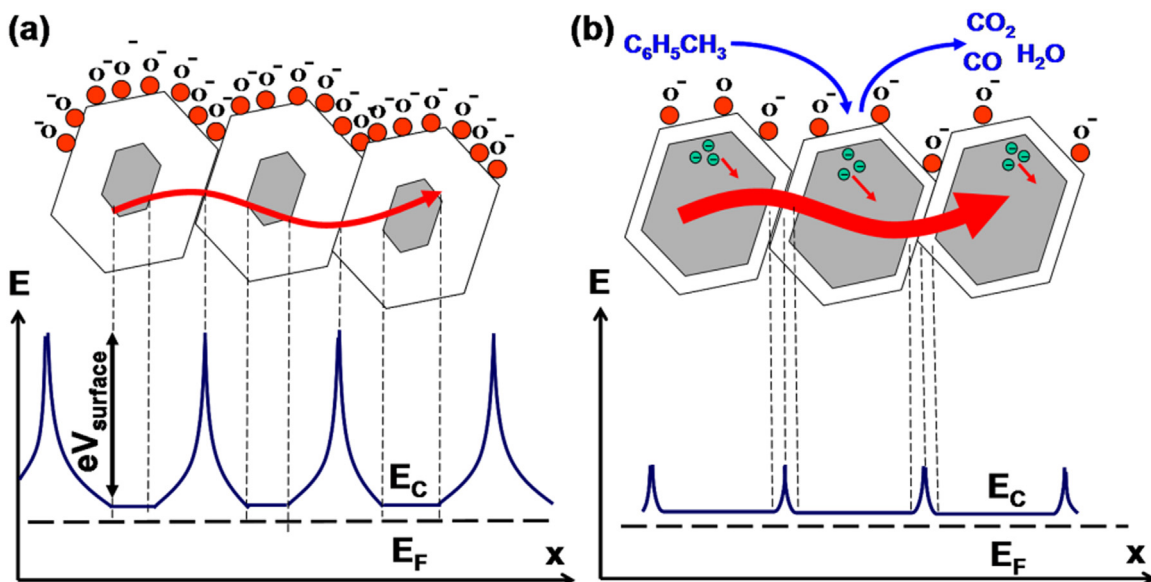
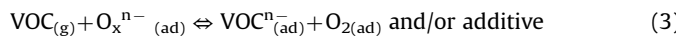
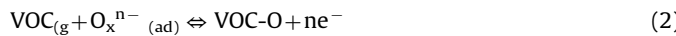


Fig. 3. Schematic energy level diagram of a metal oxide before (a) and after exposure to a VOC (b) [42].

due to the interaction with the gas molecules, do not disturb the overall conductivity of the material which will show reduced sensitivity. When the grains sizes are close to the width of the depletion region ($d \geq 2L$), the conductivity of the material begins to be affected by depleted region. It follows that, small variations in the width of space-charge layer as a result of reactions on the grains surface, leads to significant changes in conductivity. Finally, when the grains sizes are lower than the width of the depletion region ($d < 2L$), the grains can be considered fully incorporated in the space-charge layer because the whole grain is affected by the depletion of the electrons. In these conditions, the conductivity of the material is completely reliant on the charges trapped on the surface of the grains from adsorbed oxygen species, therefore, small releases of the electrons to the bulk as effect of surface reactions, will result in strong variations of the conductivity then in high sensitivity.

It worth noting that, as will be discussed below, the conductivity of a metal oxide is generally also influenced by various interfering external factors, among all the temperature and environmental humidity, therefore, the response of metal oxide based sensor is often defined as the change in electrical resistance (or a parameter related to it) when exposed to the analyte species, compared to the resistance evaluated in a reference atmosphere, typically air at specific levels of RH and temperature. On this basis, it follows that the response of such sensors to a specific analyte concentration is function of the environment where the measurement is done.

The possible sensing mechanisms of VOCs on metal oxides at a generic temperature, could be described by means of the Eq. (1) for oxygen adsorption and Eqs. (2)–(4) for VOC sensing [43,44]:



where (2) is a generic oxidation reaction of VOC which take place on the grains surface by reactive oxygen ions, (3) is the competitive adsorption of between VOC and O₂, and (4) is replacement of the adsorbed oxygen by the VOC molecules.

The type of reaction which occurs between metal oxide surface and the VOC is crucial on the response, thus on the sensitivity of the metal oxide based materials. It can be affected by many factors, such as chemical components, surface state and microstructures of sensing layers, as well as the temperature and humidity [41]. The temperature is one of the main parameters to affect the sensitivity of the material. In fact, in addition to influencing the type adsorbed oxygen species, the temperature changes the kinetic of adsorption/desorption processes for oxygen and VOC making them competitive with each other. This means that, in general, the maximum sensor response position shifts with temperature by changing the activation energy for adsorption of detected species [18]. As will be discussed below, this strategy is used to tune the sensitivity of the sensors towards a species rather than to others.

The main parameters, describing the static and dynamic features of these devices and which allow assessing the gas sensor performance, are listed below:

– *Sensitivity*. It is a parameter to evaluate the detection of the variation of the gas target concentration values in the surrounding environment. It can be considered as the change in the measurement signal per concentration unit of the gas target, in other words, it is the slope of the calibration graph.

– *Detection limit*. It is the lowest concentration value which can be detected by the sensor at definite conditions.

– *Selectivity*. It is a parameter to evaluate the property of a sensor to respond selectively to a group of gas targets or even specifically to a single one when it is present with others in the measuring environment.

– *Resolution*. It is the lowest difference of concentration which can be measured by continuously varying the gas target concentration in the mixture.

– *Response time*. It is the time required for sensor to respond to a step concentration change from zero to a certain concentration value. Usually, it is specified as the time to reach a specific ratio of the final value in the presence of target gas (usually 90%).

– *Recovery time*. It is the time that the sensor signal takes to return to its initial value after a step concentration change from a certain value to zero. Usually, it is specified as the time to reach a specific ratio of the final value (usually 90%).

– *Stability*. This is a parameter to evaluate the feature of a sensor to maintain its properties when it is continuously employed in hostile environments for a long time.

A picture of a commercial VOCs sensor is shown in Fig. 5.

It can be noted the simple design and the small size, which, together with real-time and in-situ measurements, represent a distinctive advantages of these devices with respect to other conventional gas detection techniques. The improvement of their performances for detection of some important VOCs by using nanostructured sensing materials is reviewed below.

4. Metal oxide nanostructures-based VOC sensors

4.1. Ethanol sensors

The detection of ethanol by means of sensors based on metal oxides has been extensively studied over the years. This is because ethanol is used widely in different industries and its detection and quantification in drunken drivers is very important for social security. In fact, it has been widely shown that several metal oxides with different structures, are able to detect ethanol at concentrations of a few parts per million with performance more or less relevant. Table 3 lists the ethanol sensing properties of some nanostructured metal oxide semiconductors. Among them, SnO₂ and ZnO based nanostructures show the most promising sensing performance for the monitoring of ethanol.

Mei et al. [46] synthesized 3D aloe-like SnO₂ nanostructures (Fig. 6) using a simple hydrothermal method. They reported that the developed sensor can detect ethanol at concentrations as low as 50 ppb at 285 °C with high sensitivity. The less agglomerative and thinner structure of aloe-like SnO₂ nanoparticles, together

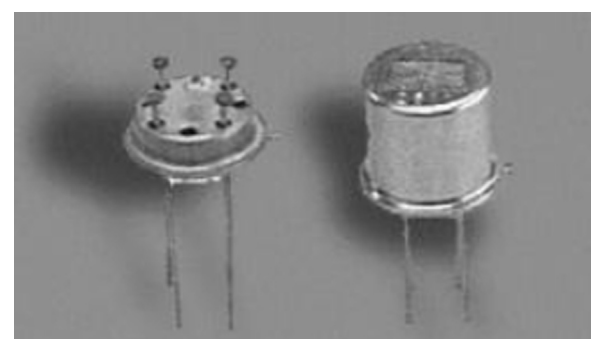


Fig. 5. Picture of a commercial VOCs sensor (Figaro TGS 2620), showing on the left the interior of the device with the sensing element and on the right the external package.

Table 3
List of metal oxide based ethanol sensors.

Material	Conc. (ppm)	Response	T (°C)	Res. time/Rec. time (s)	Refs.
Ag@Fe ₂ O ₃	100	6.3 ^a	250	5.5/16	[45]
3D aloe-like SnO ₂ nanostructures	50	25 ^b	285	1.2/76	[46]
PdO decorated-ZnO	100	35.4 ^b	320	1/7	[47]
4 wt% Pd-Ce-SnO ₂ nanoparticles	100	88 ^c	250	6/20	[48]
CoNb ₂ O ₆ NPs	120	90 ^a	130	10/18	[49]
V ₂ O ₅ NBs	1000	3.5 ^b	200	-/-	[50]
Au@In ₂ O ₃	100	36.14 ^b	160	4-2	[51]
0.2 wt% Au/In ₂ O ₃ NFs	500	13.8 ^b	140	12/24	[52]
Porous In ₂ O ₃ nanospheres	100	22 ^b	275	16/24	[53]
In ₂ O ₃ -Ag nanocomposites	1000	22 ^b	200	70/-	[54]
Co-doped In ₂ O ₃ NFs	100	16.5 ^b	300	2/3	[55]
SnO ₂ -core/ZnO-shell nanostructures	400	128 ^c	400	-/-	[56]
Ag@SnO ₂	200	2.24 ^b	RT	34/68	[57]
ZnO NTs	100	27.5 ^b	300	-/-	[58]
Ag@TiO ₂	5	4.35 ^b	RT	52/63	[59]
CuO/In ₂ O ₃ NRs	50	3.82 ^b	300	53/149	[60]
TiO ₂ NTs	5000	1.6 ^b	200	-/-	[61]
SnO ₂ NRs	300	31.4 ^b	300	1/1	[62]
Ce-SnO ₂ NPs	200	185 ^b	250	-/-	[63]
ZnO NWs	1500	61 ^b	300	-/-	[64]
TiO ₂ NBs	500	33.66 ^b	250	1/2	[65]
Ag-TiO ₂ NBs	500	41.71 ^b	200	1/2	[65]
CoFe ₂ O ₄ NPs	50	71.90 ^b	150	50/60	[66]
Co-ZnO NRs	50	9.87 ^b	350	-/-	[67]
In ₂ O ₃ NWs	100	2.00 ^b	370	10/20	[68]
In ₂ O ₃ NWs	100	2.40 ^b	275	-/-	[69]
In ₂ O ₃ NCs	69	2.70 ^b	270	-/-	[70]
In ₂ O ₃ NRs	50	115 ^b	330	6/11	[71]
In ₂ O ₃ NFs	15,000	3790 ^c	300	1/5	[72]
V ₂ O ₅ NWs	1000	9.09 ^b	330	-/-	[73]
V ₂ O ₅ NBs	100	1.7 ^b	200	32/30	[74]
Ti coated V ₂ O ₅ NBs	100	2 ^b	200	49/85	[74]
Fe coated V ₂ O ₅ NBs	100	2.3 ^b	200	36/64	[74]
Sn coated V ₂ O ₅ NBs	100	3.1 ^b	200	37/126	[74]
TeO ₂ /In ₂ O ₃ NRs	50	2.28 ^b	300	160/200	[75]
SnO ₂ NPs	250	30 ^c	100	16/25	[76]
α -Fe ₂ O ₃ NPs	100	68 ^c	325	50	[77]
1 wt% PtO ₂ -doped SnO ₂	250	100 ^b	240	23/46	[78]
0.0645SnO ₂ -0.936 α -Fe ₂ O ₃	100	230 ^c	235	-/-	[79]
0.05TiO ₂ -0.95 α -Fe ₂ O ₃	100	35 ^b	240	-/-	[79]
0.25:1 CuO/ZnO NRs	100	98.8 ^b	300	7/9	[80]
ZnO NPs	50	12.5 ^b	RT	-/-	[81]
ZnO NRs	100	3.11 ^b	300	-/-	[82]
ZnO nanorods	100	13 ^b	330	-/-	[83]
ZnO NR hollow spheres	100	80 ^b	280	-/-	[84]
Flower-like ZnO NRs	50	104.9 ^c	300	10/35	[85]
ZnO flower-like	100	14.6 ^b	300	-/-	[86]
CuO/ZnO porous flower-like	100	220 ^c	25.5	-/-	[87]
CuO andCu ₂ O nanospheres	100	2 ^b	210	-/-	[88]
CuO NCs	12.5	2.2 ^b	180	31/52	[89]
CuO NCs	10	3 ^b	200	-/-	[90]
CuO NRs	100	1.5 ^b	400	-/-	[91]
CuO NWs	1000	1.5 ^b	240	-/-	[92]
SnO ₂ /ZnO hierarchical nanostructures	25	3 ^b	400	-/-	[93]
SnO ₂ /ZnO core/shell	100	14.1 ^b	400	-/-	[94]
TiO ₂ thin film	10	13 ^c	30	65/20	[95]
SnO ₂ core-shell nanostructures	50	60 ^b	260	9/20	[96]
CdO-Fe ₂ O ₃	100	20 ^b	300	$\sim 6/\sim 10$	[97]
Pt doped SnO ₂ nanopowders	100	26.5 ^b	200	6/115	[98]
α -Fe ₂ O ₃ /ZnO nanocomposite	10	4.7 ^b	220	$\sim 20/\sim 20$	[99]
3% Nb-TiO ₂ nanorods	400	17 ^b	500	3/45	[100]
CrNbO ₄ NPs	800	66 ^c	300	-/-	[101]
ZnO NRs	100	18.29 ^b	350	$\sim 10/\sim 20$	[102]
ZnO NRs	250	2.3 ^b	280	16/120	[103]
Au modified ZnO NWs	50	7.5 ^b	325	5/20	[104]

Table 3 (continued)

Material	Conc. (ppm)	Response	T (°C)	Res. time/Rec. time (s)	Refs.
Flower-like ZnONRs	50	119 ^b	400	10/16	[105]
ZnO NRs	100	26 ^b	320	47/50	[106]
ZnO NWs	100	32 ^b	300	-/-	[107]
ZnO NBs	50	7.3 ^b	220	-/-	[108]
ZnO NTs	100	7.7 ^b	230	10/30	[109]
3%ZnO activated SnO ₂	250	57 ^b	400	10/20	[110]
TiO ₂ nanotubes	1000	1,380,000 ^d	250	90/14	[111]
10% Au-ZnO	1000	145 ^b	300	-/-	[112]
Au/ TiZnO	50	23 ^b	320	-/-	[113]
Au/ZnO	200	45 ^b	300	-/-	[114]
Flowerlike ZnO NPs	100	25.4 ^b	320	-/-	[115]
In ₂ O ₃ /Au NRs	50	42 ^b	400	9/13	[116]
α -Fe ₂ O ₃ NFs	500	12.5 ^b	250	4/600	[117]
α -Fe ₂ O ₃ NFs	500	21 ^b	225	4/1500	[117]

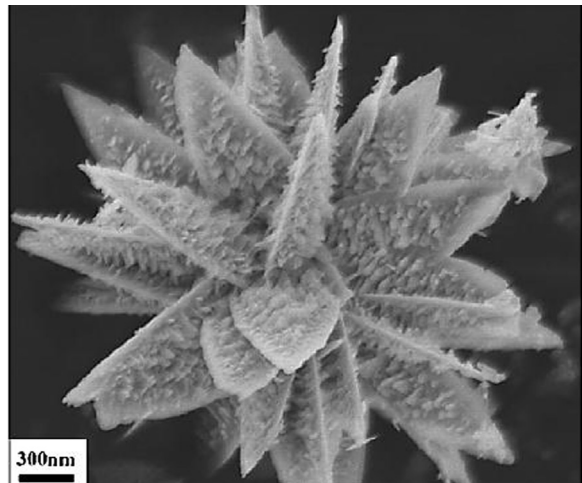
^a (R_a/R_g , %).^b (R_a/R_g or R_g/R_a , %).^c ([R_a-R_g]/ R_a , %).^d ([I_a-I_g]/ I_a).

Fig. 6. High-magnification SEM images of aloe-like SnO₂ nanostructures obtained at 550 °C [46].

with the modulation of the conductance by the small nanosheets, could be considered to explain the ultrasensitive behavior to low ethanol concentrations.

Khoang et al. [93] reported SnO₂/ZnO hierarchical nanostructures (Fig. 7) as an ethanol sensor. High-quality single crystalline SnO₂ nanowires (NW) backbones were first synthesized using the thermal evaporation method, and ZnO nanorod branches were then grown perpendicular to the axis of SnO₂ NWs via a hydrothermal approach. The ethanol sensing properties of the SnO₂/ZnO hierarchical nanostructures sensors were investigated systematically and compared with those of the bare SnO₂ NWs. The hierarchical nanostructures enhanced the ethanol gas response and selectivity in presence of interfering gases such as NH₃, CO, H₂, CO₂, and LPG. The ethanol response enhancement was attributed qualitatively to SnO₂/ZnO hetero-junctions and ZnO/ ZnO junctions considered as additional active sites.

Novel hierarchical sea urchin-like hollow core-shell SnO₂ superstructures (Fig. 8a and b) were fabricated by Liu et al. [96] employing a template-free hydrothermal method based on an inside-out Ostwald ripening mechanism. These hollow core-shell SnO₂ superstructures exhibited an almost three times stronger response to ethanol and short response and recovery times, 9 and 20 s respectively, than the hollow SnO₂ spheres (Fig. 8c and d).

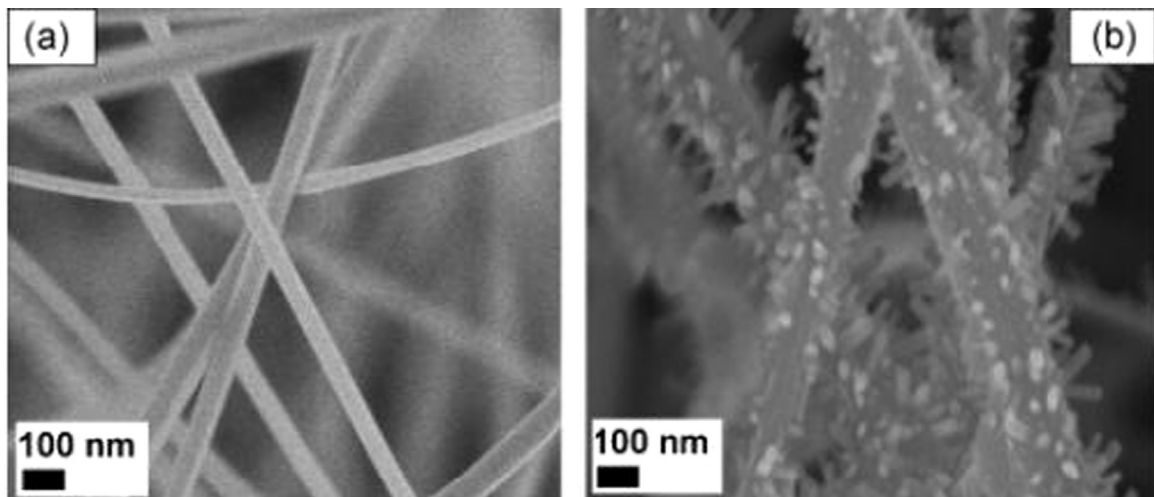


Fig. 7. SEM images of: a) bare SnO_2 nanowires, b) SnO_2/ZnO hierarchical nanostructures [93].

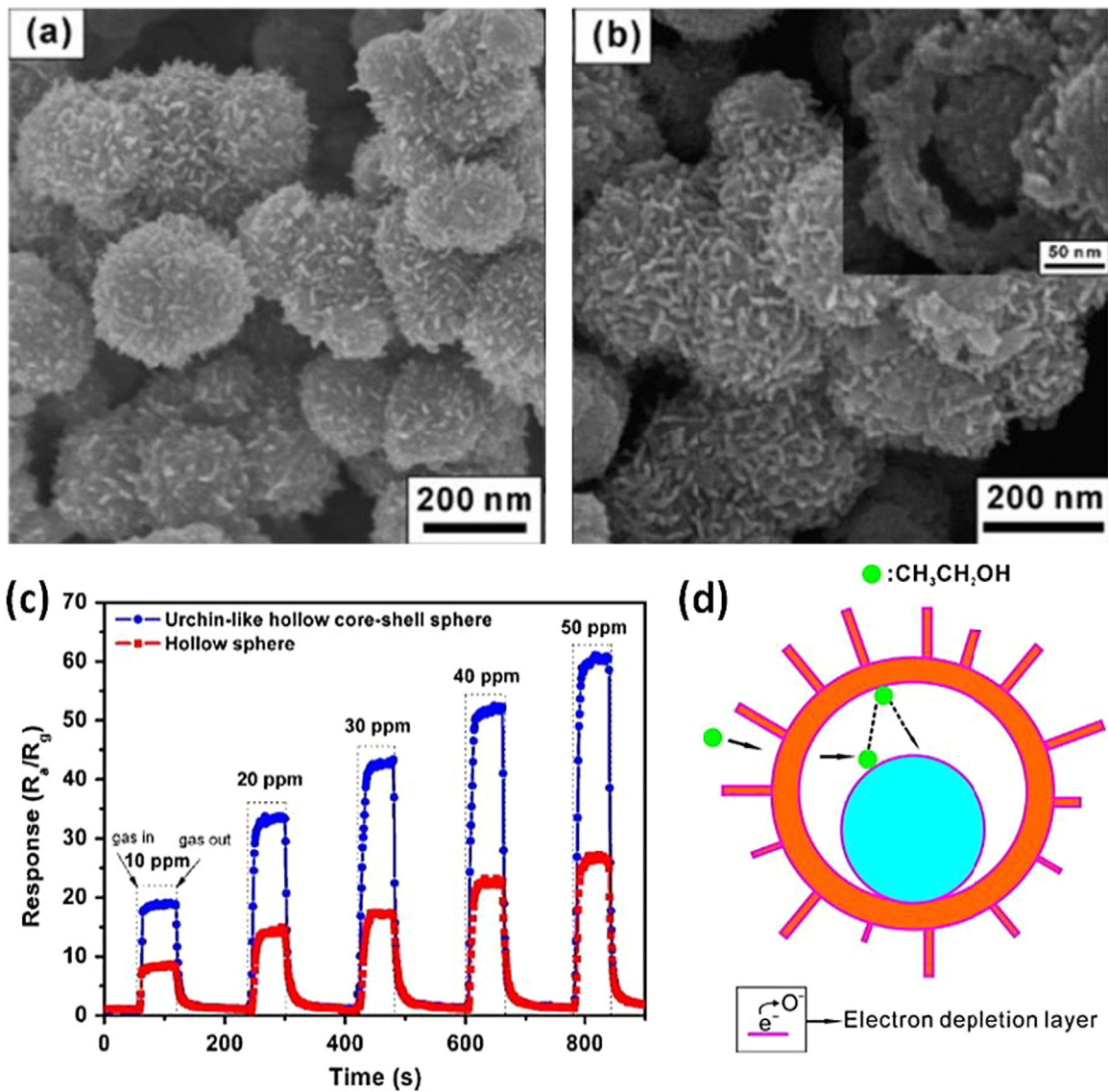


Fig. 8. a and b) SEM image of urchin-like hollow core-shell SnO_2 superstructures; c) dynamic response–recovery curves of the hollow core–shell SnO_2 superstructures and hollow SnO_2 spheres. d) Schematization of the sensing mechanism on the hollow core–shell SnO_2 superstructures [96].

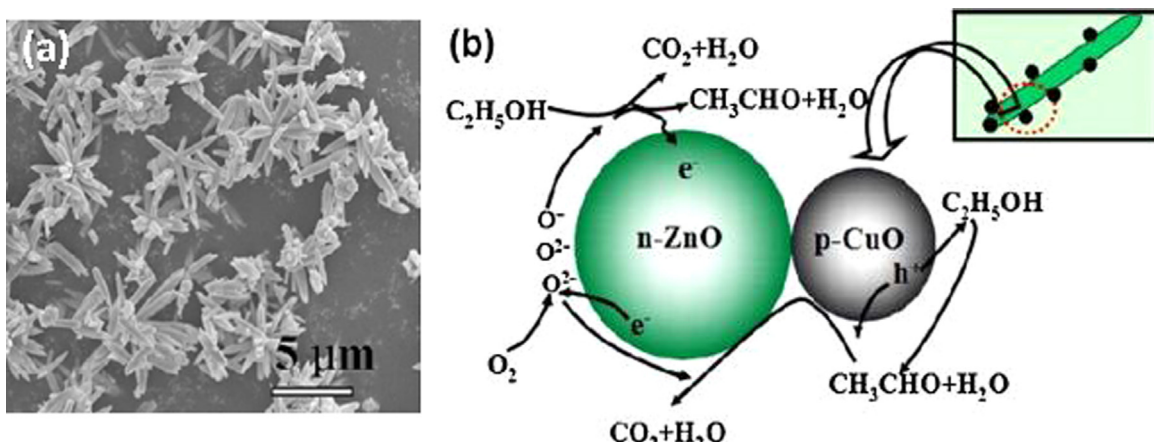


Fig. 9. a) SEM images of 0.25:1 CuO/ZnO; b) Schematic model for the 0.25:1 ZnO-CuO based sensor when exposure to ethanol [80].

Zhang et al. [80] reported a facile approach for the synthesis of flower-like p-CuO/n-ZnO heterojunction nanorods (Fig. 9). The response of the 0.25:1 CuO/ZnO nanorod sensor to 100 ppm ethanol was 98.8, which was 2.5 times that of the pure ZnO sample with response and recovery times of 7 s and 9 s, respectively. The enhanced ethanol response was attributed mainly to a wider depletion layer on the CuO/ZnO surface resulting from the formation of p-n hetero-junctions between the p-CuO nanoparticles and n-type ZnO nanorods.

New nanostructures in which metals as the core and metal oxides as the shell structure are assembled into a single metal@metal oxide core-shell nanostructure have been also investigated for high performances ethanol sensors [45]. These nanostructures not only combine the properties of both noble metals and metal oxides, but also bring unique synergistic functions in comparison with single-component materials and shows superior performances for VOCs detection [118].

4.2. Acetone sensors

Likewise ethanol case, the acetone sensors have attracted particular attention in recent years. Indeed, nowadays the monitoring of acetone, with low detection limits up to a few parts per million, has been easily achieved by means of different metal oxides. Table 4 lists the acetone sensing properties of different nanostructured metal oxides. As shown, among them, ZnO, In₂O₃ and α-Fe₂O₃ have been the most investigated sensors due to their promising potentiality for acetone detection. However, recently, it has been shown that the WO₃ is another promising metal oxide for selective and quantitative detection of acetone in ppb concentrations [119].

Righettoni et al. [119] synthesized pure and Si-doped WO₃ nanoparticles (Fig. 10) to fabricate chemosensors utilized for quantitative analysis of acetone in ideal (dry air) and realistic (90% RH) conditions.

The acetone sensor response (4.63 for 600 ppb) at 400 °C in dry air was compared to that of water vapor (0.7 at 90% RH) and ethanol (0.97 for 600 ppb), demonstrating high acetone selectivity. However, increasing RH to 90% decreased the response to 68% of that for 600 ppb in dry air, indicating a relevant effect of humidity in reducing the sensitivity. Anyway, the rapid response to 20 ppb of acetone at such RH conditions was demonstrated.

Kim et al. synthesized pristine WO₃, Au decorated, Pd decorated and Au/Pd-decorated WO₃ nanorods (Fig. 11) for acetone sensing [120].

In the case of WO₃ nanorods coated with Au or Pd-monometallic catalyst nanoparticles, the enhanced sensitivity was based on the excellent Au or Pd ability of catalytic dissociation of both

Table 4
List of metal oxide based acetone sensors.

Material	Conc. (ppm)	Response	T (°C)	Res. time/Rec. time (s)	Refs.
Si-WO ₃ nanoparticles	0.6	4.63 ^a	400	350	[119]
WO ₃ nanorods	200	108.25 ^a	300	237	[120]
Pd-WO ₃ nanorods	200	138.62 ^a	300	120	[120]
Au-WO ₃ nanorods	200	131.26 ^a	300	98	[120]
AuPd-WO ₃ nanorods	200	152.4 ^a	300	101	[120]
Ce-SnO ₂ hollow spheres	100	12 ^b	250	40	[121]
4 at% Ce-doped α-Fe ₂ O ₃ nanotubes	50	21 ^b	240	3	[122]
1 wt% Pt/γ-Fe ₂ O ₃	1	75 ^c	250	~10	[123]
7 wt% La-doped α-Fe ₂ O ₃ nanotubes	50	26 ^b	240	3	[124]
Ce-doped CoFe ₂ O ₄	2000	157 ^a	200	38	[125]
SnO ₂ nanoparticles	90	3.75 ^b	200	~10	[126]
ZnO nanorods	100	30 ^b	300	~5	[127]
Sn-doped ZnO	400	130 ^a	300	-/	[128]
ZnO-TiO ₂	100	52.5 ^b	370	10	[43]
Hollow SnO ₂ /α-Fe ₂ O ₃ spheres	10	2.5 ^b	250	-/	[129]
Single-crystalline WO ₃ nanoplates	500	36 ^b	200	3/6	[130]
In ₂ O ₃ NWs	25	7 ^b	400	-/	[131]
Sparked In ₂ O ₃ film	2000	117 ^b	350	-/	[132]
1 wt% PbO doped SnO ₂	N/A	92.6 ^c	250	-/	[133]
Nanocrystalline ZnO	2000	92 ^c	350	-/	[134]
3D aloe-like SnO ₂ nanostructures	50	6.5 ^b	240	-/	[46]
α-Fe ₂ O ₃	100	10 ^b	300	34/44	[135]
α-Fe ₂ O ₃ -Au	100	20 ^b	260	26/24	[135]
α-Fe ₂ O ₃ -ZnO	100	43 ^b	250	19/20	[135]
α-Fe ₂ O ₃ -Au-ZnO	100	113 ^b	225	17/13	[135]
α-Fe ₂ O ₃ @ZnO core-shell	100	280 ^b	12	-/	[136]
α-Fe ₂ O ₃ @ZnO core-shell	100	8 ^b	370	-/	[137]
Au-α-Fe ₂ O ₃ nanorods	100	45 ^b	270	-/	[138]
α-Fe ₂ O ₃ -ZnO nanorods	100	28 ^b	225	-/	[139]
α-Fe ₂ O ₃ -Au nanospindles	100	7.2 ^b	300	-/	[140]
α-Fe ₂ O ₃ @SnO ₂ -Au	100	2.3 ^b	320	-/	[141]
In ₂ O ₃ /Au NRs	50	38 ^b	250	10/18	[116]
In ₂ O ₃ /Pt NPs	1.56	12 ^b	200	25/120	[40]

^a (R_a/R_g, %).

^b (R_a/R_g).

^c ([R_a-R_g]/R_a, %).

oxygen and acetone molecules. In the case of WO₃ nanorods decorated with Au/Pd bimetallic catalyst nanoparticles, the enhanced sensitivity might be attributed to the synergistic effect due to modification of the electronic structure of the Pd-Au nanoalloys, which improves the adsorption and activation of the target gas species on the material surface.

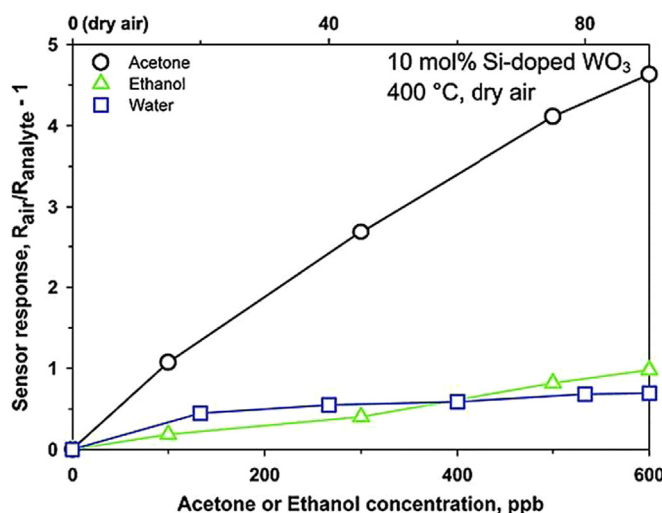


Fig. 10. Sensor response to acetone (circles), water (squares), and ethanol (triangles) vapors [119].

Karmaoui et al. [40] reported the high sensitivity of sub-spherical $\text{In}_2\text{O}_3/\text{Pt}$ nanoparticles for detecting ppb levels of acetone. By a novel non-aqueous sol gel route the authors synthesized monodispersed and homogeneous In_2O_3 NPs with diameters of 6–8 nm, decorated with ultrafine Pt NPs (2–3 nm) on their surface. The advantage of this preparative process was that it preserved metallic platinum NPs formed during the synthesis. An acetone sensor based on these materials was fabricated which showed extreme high sensitivity and lower detection limit as low as 10 ppb, which is one of the lowest detection limit ever reported for any chemoresistive acetone sensors. Furthermore, although the humidity had adverse effect on the sensitivity, the sensor showed high response at ppb acetone levels also in presence of RH higher than 75%. The authors ascribed these exceptional performances to the key role played by very small Pt metal NPs uniformly distributed on the likewise small In_2O_3 NPs.

4.3. Formaldehyde sensors

As stated before, formaldehyde is highly toxic volatile compound and has been classified as a human carcinogen that causes nasopharyngeal cancer and probably leukemia. Therefore, many

Table 5
List of metal oxide based formaldehyde sensors.

Material	Conc. (ppm)	Response	T (°C)	Res. time/Rec. time (s)	Refs.
$\gamma\text{-Fe}_2\text{O}_3$ nano powder	100	6 ^b	320	–	[143]
MWCNTs-doped nano SnO_2	50	4 ^b	250	–	[144]
LaFeO_3 hollow nanospheres	500	20 ^b	260	13/25	[145]
Au@SnO_2	50	2.9 ^b	RT	80/69	[146]
Nano ZnO	1000	997 ^b	210	10/20	[147]
10 mol% CdO-2.2 mol% Sn doped ZnO	200	2000 ^b	200	less than 300	[148]
$\text{CdO-In}_2\text{O}_3$	10	100 ^b	95	120/240	[149]
Cd-doped $\text{TiO}_2\text{-SnO}_2$ composites	100	15 ^b	320	–/-	[150]
1.0 wt% $\text{MnO}_2\text{-ZnO}$	200	27 ^b	320	27/12	[151]
1 mol% Pd-doped SnO_2	10	1.55 ^b	250	50/50	[152]
$\text{SnO}_2\text{-NiO}$	0.3	18 ^c	300	–/-	[153]
ZnO nanorods	50	11.7 ^d	UV assisted	–/-	[154]
Ga-doped ZnO	205	13 ^a	400	30/210	[155]
NiO	10	1.5 ^b	300	13.2	[156]
NiO	20	4.3 ^b	340	420	[157]
SnO_2 -nanowires	10	2.45 ^b	270	90/150	[158]
Ga-doped ZnO	205	13 ^a	400	30/210	[155]
Au@ZnO	5	10.57 ^b	RT	138/104	[159]
La_2O_3 -sensitized SnO_2	18.7	55 ^b	250	–/-	[160]
Ag-LaFeO_3	1	25 ^b	90	65/60	[161]
$\text{SnO}_2\text{/In}_2\text{O}_3$ hetero-nanofibers	10	7.5 ^b	375	–/-	[162]
$\text{La}_{1-x}\text{Sr}_x\text{FeO}_3$ nanoparticles	50	26 ^b	200	260/70	[163]
Hollow $\text{SnO}_2\text{/}\alpha\text{-Fe}_2\text{O}_3$ spheres	10	2 ^b	250	–/-	[129]
Cd-loaded In_2O_3 hollow nanofibers	10	16 ^b	280	160/70	[164]
$\alpha\text{-Fe}_2\text{O}_3$ nanoparticles	100	52 ^c	325	180	[77]
Mesoporous worm-like SnO_2 NPs	10	100 ^b	150	–/-	[165]

^a (R_a/R_g , %).

^b (R_a/R_g or R_g/R_a).

^c ($(|R_a-R_g|)/R_a$, %).

^d ($(|I_a-I_g|)/I_a$)

works have been addressed to develop new sensors able to detect its presence in both industrial and residential environments [142]. As shown in Table 5, different metal oxides have been investigated

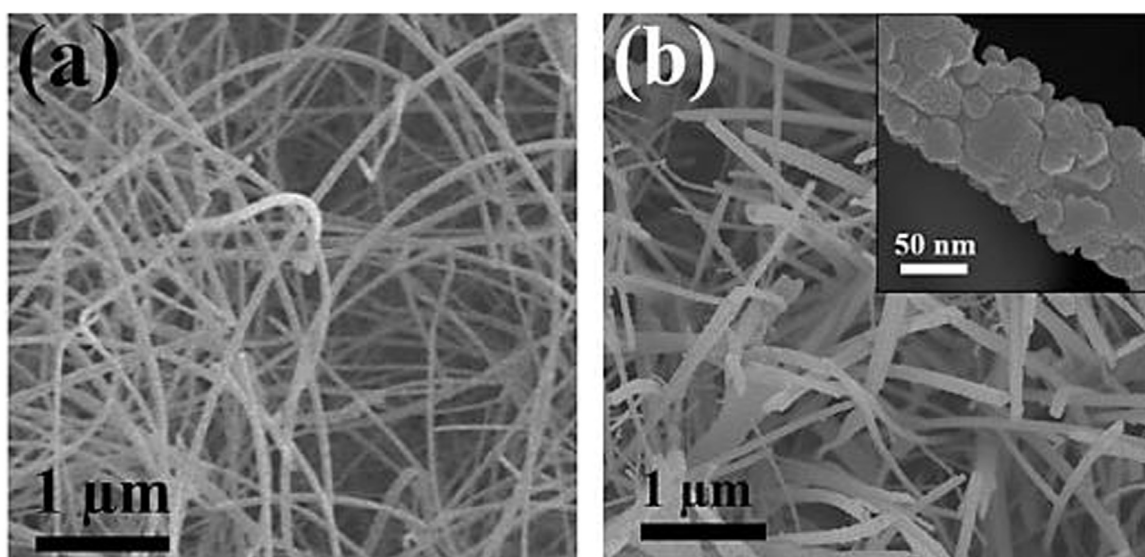


Fig. 11. (a) SEM image of pristine WO_3 nanorods and (b) Au/Pd-decorated WO_3 nanorods [120].

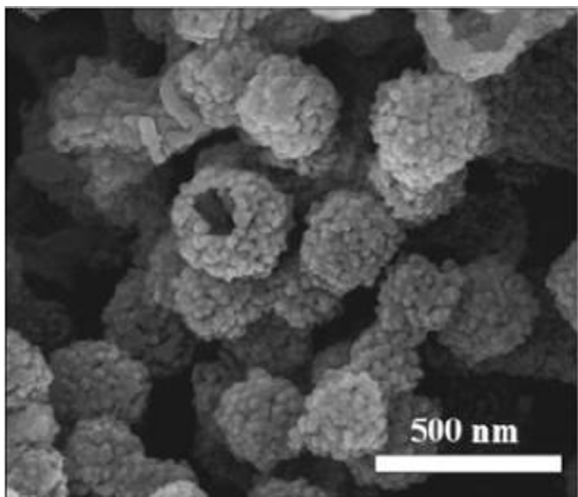


Fig. 12. SEM image of LaFeO_3 hollow nanospheres [145].

to detect formaldehyde. Among them, ZnO , WO_3 , NiO , hybrid materials and perovskite oxides have shown excellent sensitivity towards this analyte.

Zhang et al. [145] synthesized perovskite-type LaFeO_3 hollow nanospheres using carbon spheres as templates (Fig. 12). They tested these nanospheres for the detection of formaldehyde (20–2000 ppm) and reported a relatively good response ($R_g/R_a=13$ for 200 ppm at 260 °C). They attributed the superior gas sensing

performance of nanospheres towards formaldehyde to their porosity, large surface area then more active sites, conferred by the hollow structure.

Han et al. [148] reported a new hybrid material for formaldehyde detection based on a combination of CdO and Sn-doped ZnO . As first, they showed that Sn dopant (2.2 mol%) can effectively increase the formaldehyde response of ZnO sensor compared to the other dopants. Moreover, CdO activated ZnO based formaldehyde gas sensing material, and 10 mol% CdO activated 2.2 mol% Sn-doped ZnO showed the highest formaldehyde sensitivity with high linear sensitivity at 200 °C.

Peng et al. [154] examined the formaldehyde sensing properties of ZnO nanorods under UV illumination. They reported that under UV illumination the response to formaldehyde is enhanced than in its absence. The mechanism of gas sensing under UV light irradiation is discussed as follows: Under UV light irradiation, a large number of photo-generated electrons and holes exist in ZnO . The adsorbed oxygen ions can be neutralized with the photo-generated holes and then reacts with the photo-active formaldehyde molecules. As a result, the number of photo-generated holes and oxygen adsorbed on the nanorods decreases strongly upon the reaction. Therefore, an increase in conductivity by photo-catalytic formaldehyde oxidation arises from three aspects. First, the amount of consumed photo-generated holes is more than that of the photo-generated electrons. Second, the number of trapped electrons is reduced remarkably on the nanorods surface, due to a decrease in the oxygen adsorbed. Third, the interface potential barrier height is decreased for the consumption of the adsorbed oxygen.

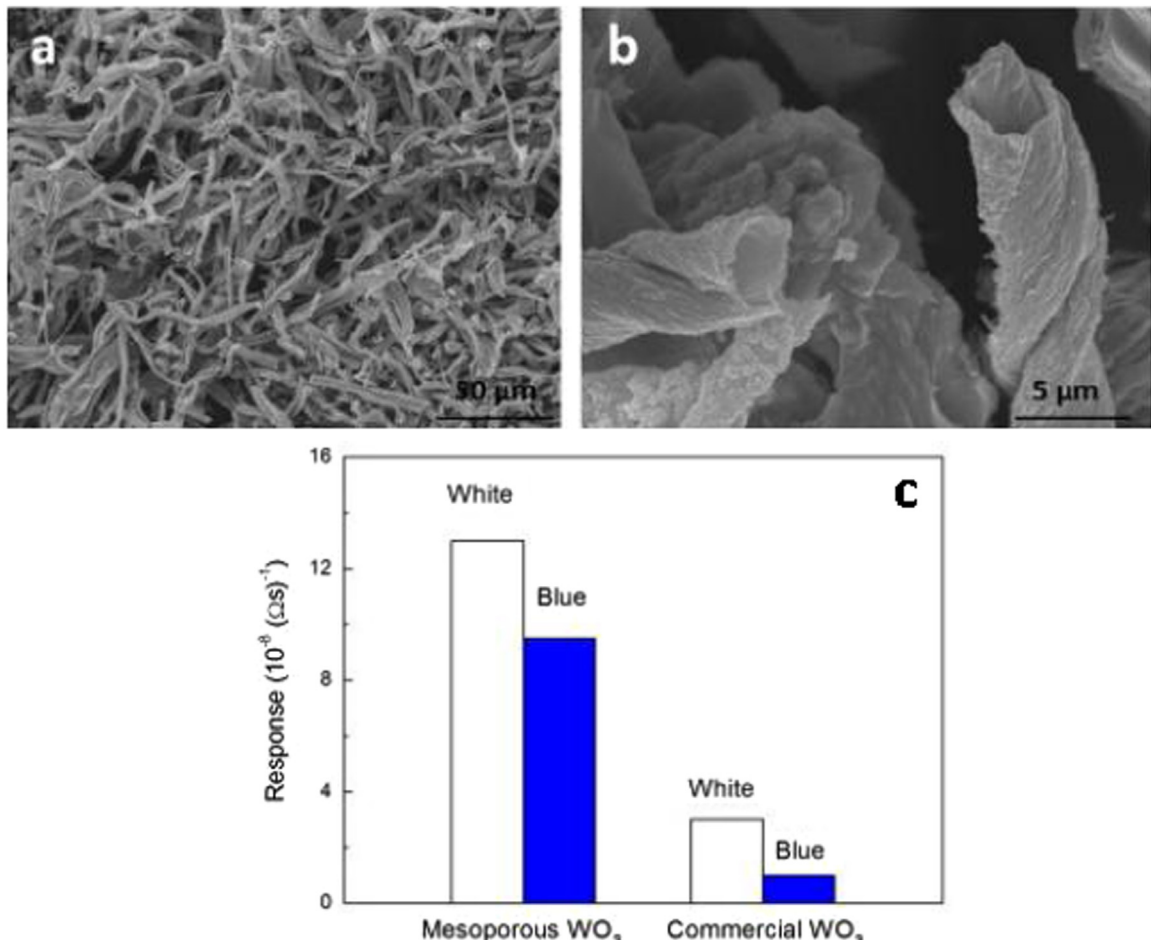


Fig. 13. a and b) SEM images of the mesoporous WO_3 ; c) responses of WO_3 sensors to formaldehyde (100 ppm) activated by white light and blue light [162]. (For interpretation of the references to color in this figure legend, the reader is referred to the web version of this article.)

Castro-Hurtado et al. [157] examined the effects of the NiO film thickness on the formaldehyde sensitivity. They revealed that 150 nm thick film sensors have better sensing responses compared to 300 nm thick film sensors. In fact, they showed that the response to 5 ppm of formaldehyde for the first one samples was two times stronger than that of the second ones probably due to the smaller grain size.

Deng et al. [166] investigated the sensing properties of a commercial and mesoporous WO_3 (Fig. 13a and b) for formaldehyde detection at room temperature under visible light.

The gas sensing properties of mesoporous WO_3 was greater than commercial one, which can be attributed to the larger surface area, the presence of the mesopores and the increased absorbance to visible light. The larger surface area, due to the mesoporous structure, enhanced the amount of O^{2-} providing more reacting sites. An increase in absorbance to visible light (Fig. 13c) could improve the performance due to the formation of photogenerated $\text{O}^{2-}(\text{h}\nu)$.

4.4. Toluene sensors

Over the past few years, extensive attention has been paid to the development of toluene sensors using nanostructured metal oxide semiconductors. As shown in Table 6, different structures based on ZnO have often been used effectively for the detection of toluene. Furthermore, excellent sensing properties have been proven for mesoporous cobalt oxide (Co_3O_4) in the motoring of this VOC.

Lou et al. [47] examined the toluene sensing properties of flower-like pristine (ZnO) and PdO-decorated ZnO (PdO-ZnO) materials with a hierarchical structure synthesized via a surfactant-free hydrothermal route (Fig. 14a).

They reported that the PdO-ZnO sensor exhibited a response towards toluene approximately 4–5 times higher than that of pristine ZnO at the optimal operating temperature of 240 °C (Fig. 14b and c). This might be due to the well-aligned hierarchical

structures and the incorporation of an interface between the ZnO rods and PdO nanoparticles grown on the ZnO. They hypothesized that, with the assistance of PdO, oxygen molecules could be adsorbed more easily at the surface of the ZnO rods. This process increases both the quantity of adsorbed oxygen and the molecule-ion conversion rate, resulting in a greater and faster degree of electron depletion from the ZnO rods. Therefore, the response of the PdO-decorated ZnO rods is distinctly higher than pristine ZnO.

Zeng et al. [171] reported the preparation via a hydrothermal route, of the large-scale flowerlike pure and TiO_2 doped ZnO nanostructures consisting of many aggregative nanorods with a diameter of about 60 nm (Fig. 15a). The toluene sensing properties of the pure ZnO and TiO_2 -doped ZnO nanostructures were tested at different operating temperatures from 160 to 390 °C, and toluene concentrations ranging from 1 to 100 ppm (Fig. 15b). The TiO_2 -doped ZnO sensor exhibited a remarkably enhanced response, faster response and recovery times than that of un-doped ZnO, as well as the low operating temperature.

Liu et al. [172] synthesized fiber-like mesoporous Co_3O_4 by a nanocasting method using mesoporous silica (SBA-15) as hard template and $\text{Co}(\text{NO}_3)_2 \cdot 6\text{H}_2\text{O}$ as cobalt source. They showed that, compared to its non-porous counterparts, mesoporous Co_3O_4 has very good response to toluene in the range 1–1000 ppm. Furthermore, mesoporous Co_3O_4 also exhibited high selectivity for detection of toluene, compared to other interfering VOCs, such as ethanol, formaldehyde, ethanol, acetone, methanol and ammonia.

4.5. Methanol sensors

The wide ranges of applications, toxicity and clinical implications of methanol have made necessary to develop reliable and high performance methanol sensors. Table 7 lists the methanol sensing properties of some nanostructured metal oxide semiconductors. As it is observable, besides the common metal oxides based on SnO_2 , ZnO , In_2O_3 and $\alpha\text{-Fe}_2\text{O}_3$, some ferrite-type perovskites have shown excellent sensitivity towards methanol detection.

Han et al. synthesized pristine and Ce-doped In_2O_3 porous nanospheres (Fig. 16a) by a hydrothermal method [180]. Compared with pure In_2O_3 samples, Ce-doped In_2O_3 porous nanospheres showed excellent sensing performance towards methanol at 320 °C (Fig. 16b) and improved long term stability.

Three main factors were mentioned for improving gas sensing properties of Ce-doped sensors: first, the crystallite size was considerably reduced by the incorporation of Ce element then the high specific surface area provides more active sites for oxygen molecules adsorbed on its surface; second, Ce doping effectively influences the electronic properties of In_2O_3 releasing electrons into the conduction bound, which increased the concentration of free electrons; finally, due to ability of ceria to take and release oxygen under oxidizing and reducing conditions, could favor more oxygen adsorption then increasing the response.

Yang et al. [192] prepared hematite ($\alpha\text{-Fe}_2\text{O}_3$) hollow spheres by a one-step hydrothermal reaction without template and used it to fabricate the a methanol gas sensor. The sensor exhibited excellent sensing performance to methanol at 280 °C, with a response (R_a/R_g) of 25 for 10 ppm methanol and fast response and recovery time of 8 and 9 s respectively. In addition the lowest detection limit reached was 1 ppm with the response value of 2.5, while a good selectivity to methanol was ensured in presence of similar VOCs.

Qin et al. [186] synthesized three-dimensional ordered macroporous perovskites ($\text{La}_{1-x}\text{Mg}_x\text{FeO}_3$) by a simply PMMA template method (Fig. 17).

The $\text{La}_{0.95}\text{Mg}_{0.05}\text{FeO}_3$ based-sensor showed the highest gas response towards methanol at 190 °C. In addition, it showed

Table 6
List of metal oxide based toluene sensors.

Material	Conc. (ppm)	Response	T (°C)	Res. time/ Rec. time (s)	Refs.
PdO decorated-ZnO	100	10.9 ^a	240	1/9	[47]
$\text{Fe}_3\text{O}_4\text{-NiO}$ core-shell nanostructure	100	13 ^a	280	27	[167]
Sm FeO_3 NPs	3	12 ^a	400	-/-	[44]
Hollow $\text{SnO}_2/\alpha\text{-Fe}_2\text{O}_3$ spheres	10	2.3 ^a	250	-/-	[129]
Pd-NPs/Pd-embedded WO_3 NFs	10	5 ^a	350	10.9/16.1	[168]
MnO-Indium Tin Oxide ($\text{In}_2\text{O}_3\text{:}10\%$ SnO_2) thin films	1000	85 ^b	227	45/52	[169]
Ni doped ZnO	5	25 ^a	400	-/-	[170]
TiO_2 -doped flowerlike ZnO	50	11 ^a	290	15/25	[171]
Mesoporous Co_3O_4	100	23.55 ^a	190	233/165	[172]
Monodisperse Co_3O_4 nanocubes	100	4.8 ^a	200	-/-	[173]
Co_3O_4 hollow nanospheres	1000	8 ^a	100	-/-	[174]
$\text{SnO}_2\text{-Fe}_2\text{O}_3$ nanotubes	50	25.3 ^a	260	-/-	[175]
NiO- SnO_2 composites	50	11 ^a	330	11.2/4	[176]
Tetrapod-shaped ZnO	100	7 ^a	380	50/20	[177]
TiO_2 nanotubular	500	53 ^a	500	110–130/800–1150	[178]
Hierarchical meso-macro-porous SnO_2	100	3 ^a	220	7/36	[179]
V_2O_5 nanowires	1000	2 ^a	330	-/-	[73]

^a (R_a/R_g).

^b ([$R_a\text{-}R_g$]/ R_a , %).

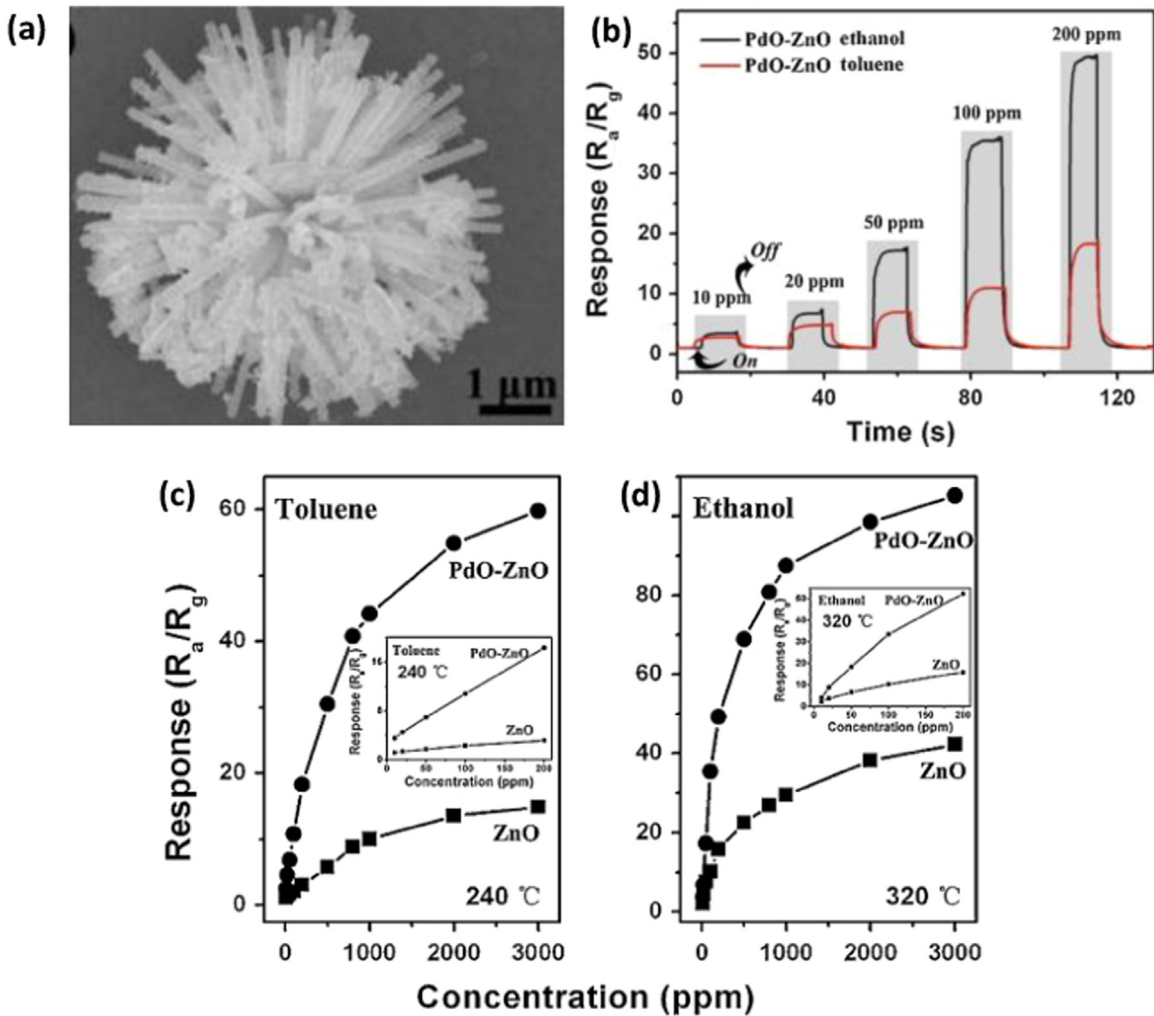


Fig. 14. a) SEM images of flower-like PdO-ZnO; b) dynamic responses to ethanol and toluene of PdO-ZnO at 320 °C; c-d) calibration curves of both PdO-ZnO and ZnO towards toluene and ethanol concentrations at 240 °C and 320 °C, respectively [47].

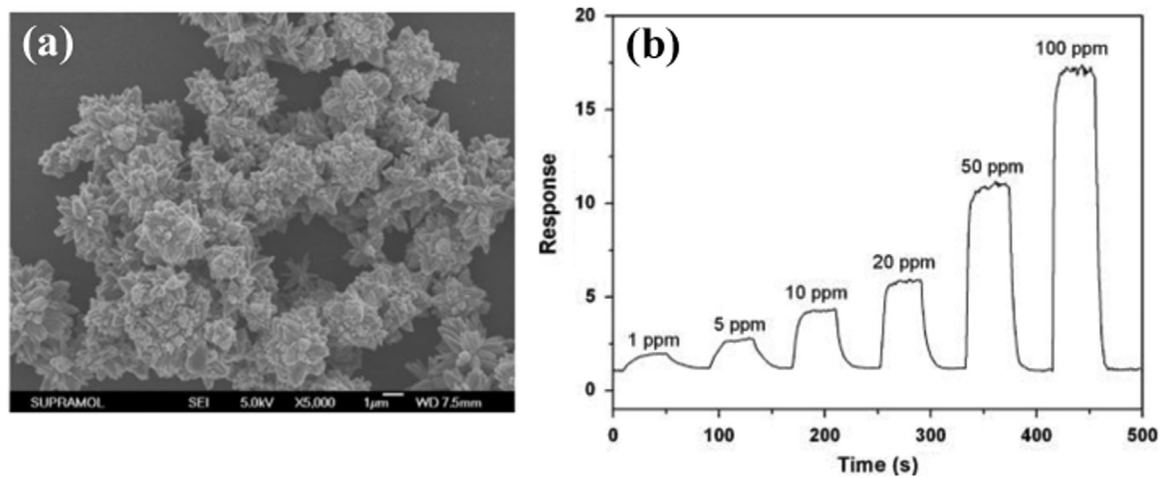


Fig. 15. a) Micrograph of TiO₂-doped ZnO nanorods; b) Response of doped ZnO versus toluene concentrations at 290 °C [171].

excellent selectivity to methanol compared to other VOCs. They attributed this enhancement in gas sensing properties not only to its ordered macro-mesoporous structure, but also to the doping of Mg²⁺ that significantly enhanced the gas sensing properties combining the effect of electrovalence compensation and oxygen vacancy compensation.

4.6. Acetylene sensors

Acetylene is a combustible and highly explosive gas. Therefore, considerable efforts are needed to fabricate practical acetylene sensors and on how to enhance their gas sensing properties further. The acetylene sensing performances reported so far require

Table 7
List of metal oxide based methanol sensors.

Material	Conc. (ppm)	Response	T (°C)	Res. time/Rec. time (s)	Refs.
3 wt% PbO doped SnO ₂	1000	69.5 ^b	350	-/-	[133]
SmFeO ₃ NPs	3	26 ^a	400	-/-	[44]
Ce-doped In ₂ O ₃ nanospheres	100	35.2 ^a	320	14/10	[180]
La _{0.8} Pb _{0.2} FeO ₃ NPs	200	50 ^b	230	40/75	[181]
Co ₃ O ₄ -intercalated reduced graphene oxide	800	8.5 ^a	RT	240/360	[182]
CdS-doped SnO ₂ thick films	5000	70 ^a	200	40/110	[183]
Al-doped ZnO thin films	500	44 ^b	275	280/-	[184]
CuO thin films	500	12 ^b	350	380/-	[185]
La _{1-x} Mg _x FeO ₃	100	150 ^a	190	-/-	[186]
La _{1-x} Ba _x FeO ₃	500	11 ^a	240	-/-	[187]
LaCo _x Fe _{1-x} O ₃	500	45 ^a	120	-/-	[188]
porous LaFeO ₃	500	4.2 ^a	240	-	[189]
La _{1-x} Sr _x FeO ₃ NPs	50	10.5 ^a	200	-/-	[163]
SnO ₂ porous nanosheets	50	3 ^a	300	-/-	[190]
Hollow SnO ₂ /α-Fe ₂ O ₃ spheres	10	2.2 ^a	250	-/-	[129]
Single-crystalline WO ₃ nanoplates	500	105 ^a	200	-/-	[130]
Cd-loaded In ₂ O ₃ hollow nanofibers	30	3.8 ^a	280	-/-	[164]
SnO ₂ /In ₂ O ₃ hetero-NFs	50	2 ^a	375	-/-	[162]
Flower like ZnO NPs	100	13.8 ^a	320	-/-	[115]
SnO ₂ thin film	10,000	21 ^a	250	-/-	[191]
Hollow α-Fe ₂ O ₃ spheres	10	25 ^a	280	8/9	[192]

^a (R_a/R_g).^b ([R_a-R_g]/ R_a , %).

significant improvement, such as high response, short response and recovery time, selectivity, and stability [193]. Few reports have been devoted to the use of metal oxides for the detection of acetylene in comparison to other VOCs previously discussed and, as shown in Table 8, most of them concern the use of ZnO.

Tamaekong et al. [194] used Pd-loaded ZnO nanoparticles as acetylene sensors. The fabricated sensors showed good sensing behavior towards C₂H₂. They attributed the strong response to the catalytic effect of Pd. This catalyst enhances the reducing gas sensing of metal oxide via a spillover mechanism. This interaction is a chemical reaction through which additives assist the redox

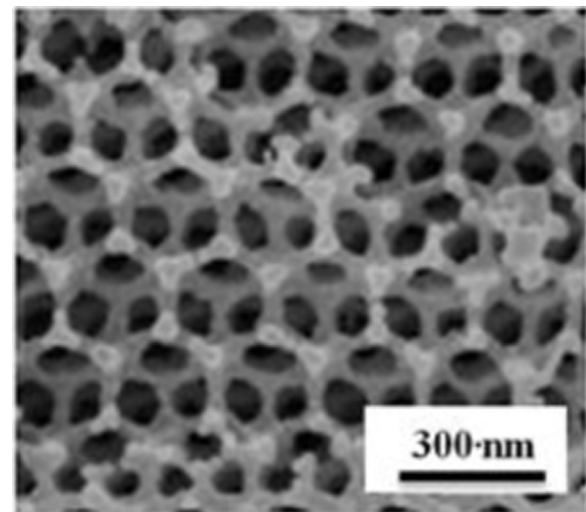


Fig. 17. SEM image of La_{0.95}Mg_{0.05}FeO₃ macroporous perovskites [186].

Table 8
List of metal oxide based acetylene sensors.

Material	Conc. (ppm)	Response	T (°C)	Res. time/Rec. time (s)	Refs.
Pt loaded ZnO	10,000	836 ^a	300	6/60	[194]
5% Ni-doped ZnO	2000	17 ^a	250	5/10	[195]
6 wt% Sm ₂ O ₃ -doped SnO ₂	1000	65 ^a	180	4/16	[196]
ZnO NPs	5000	15 ^a	220	-/-	[197]
5 wt% Ag/ZnO Hrc-RGO	100	12.3 ^a	200	57/90	[198]
Ag/ZnO NPs-decorated RGO	100	21.2 ^a	150	25/80	[199]
ZnO/RGO	100	18.2 ^a	250	100/24	[200]

^a (R_a/R_g).

process of metal oxides. The term spillover refers to the process where the metal catalysts dissociate the molecules to atoms which can then 'spillover' onto the surface of the semiconductor support. At the appropriate temperatures, the reactants are first adsorbed on to the surface of the additive particles and then migrate to the

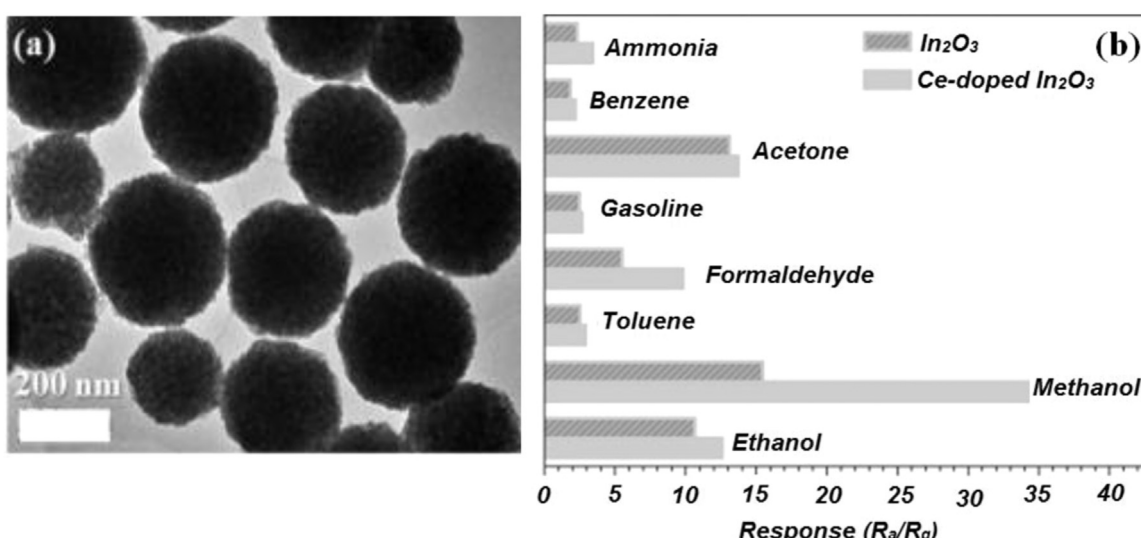


Fig. 16. TEM image of Ce-doped In₂O₃ porous nanospheres; b) Sensors response of pure and Ce-doped In₂O₃ sensors to 100 ppm of ammonia, benzene, toluene, methanol, formaldehyde, ethanol, and methanol at 320 °C [180].

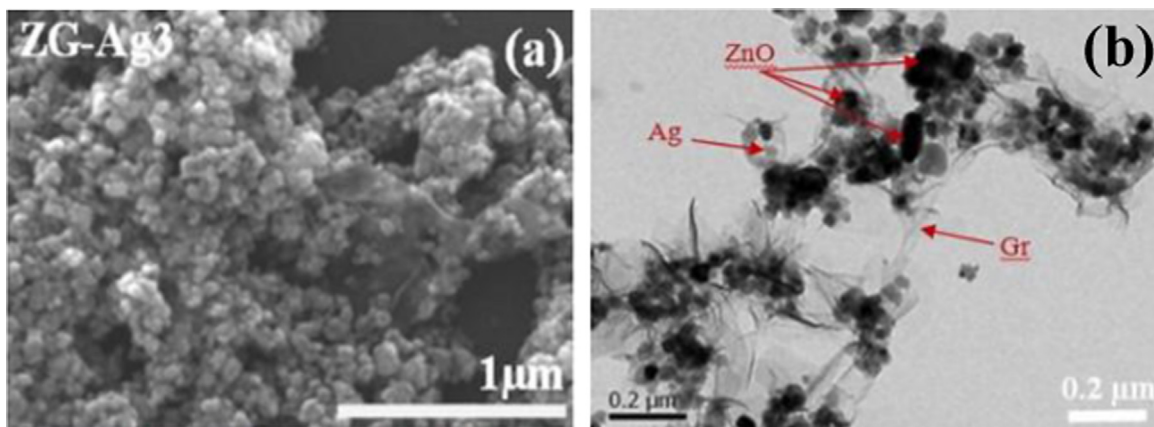


Fig. 18. Morphological characterization of Ag-loaded ZnO/ rGO. a) SEM micrograph; b) TEM micrograph [199].

oxide surface to react with surface oxygen species, affecting the surface conductivity.

ZnO/reduced graphene oxide (rGO) and Ag-loaded ZnO/ rGO hybrid nanostructures (Fig. 18) as sensitive materials for low temperature acetylene detection were recently investigated by Uddin et al. [199,200].

At optimum conditions (150 °C, 3 wt% Ag-loaded ZnO/rGO) the as-synthesized hybrid nanostructure showed enhanced sensing properties towards acetylene compared with Ag-free counterpart such as a high response of 21.2 (R_a/R_g) for 100 ppm of acetylene, an acceptable detection range of 1–1000 ppm, excellent repeatability, fast response/recovery times of 25/80 s, good selectivity and performance stability up to 31% RH concentration.

4.7. Benzene sensors

Although benzene is known for its high toxicity and carcinogenic properties, and its presence in the atmosphere is very frequent because of the different human activities that produce it, only very few works have been devoted to the exclusive monitoring of this VOC. In Table 9 are listed some of the most relevant metal oxide based sensors for the detection of benzene.

Zhu et al. [43] reported a highly sensitive VOCs sensor based on mixed ZnO-TiO₂ nanoparticles. They obtained excellent sensitivity towards benzene detection with very fast response and recovery times working at 370 °C. In particular they found that the gas sensing properties of ZnO-TiO₂ mixed thick films depend on the TiO₂ content affecting the gas sensitivity by modifying their phase structure, microstructure and conductivity. Additions of 5–10% TiO₂ distinctly decreased the grain size leading to fairly good

sensing performance to VOCs in air, in the range of 10–200 ppm at 370 °C with an increase in TiO₂ content. Although the realized sensor showed excellent sensitivity to benzene it had poor selectivity against other VOCs such as acetone and ethanol.

Wang et al. [202] synthesized a novel Cu₂O octahedral nanostructure (Fig. 19a) and investigated their sensing performance towards benzene and NO₂. Comparing Cu₂O octahedral nanostructure and Cu₂O nanorods (Fig. 19b), they observed an enhanced sensitivity and high selectivity towards benzene for the first one structure. Working at 230 °C they obtained a response (R_a/R_g) close to 10 with very short response and recovery times of 3 and 4 s, respectively (Fig. 19c and d). Furthermore they showed the possibility to use the same material to monitor NO₂ by working at low temperature (50 °C) thanks to the high sensitivity and selectivity towards the last gaseous specie at above conditions.

Vaishnav et al. [204] developed an ITO thin film sensor for detection of benzene, furthermore, in order to enhance the sensor performance, different sensors with thin promoting layers of Cr, MnO, MgO and Cu, deposited on the top of the surface of ITO were fabricated and tested. It was observed that the sensor with Cr layer on ITO shows maximum relative change in resistance of the film suggesting more sensitivity. This might be mainly due to the high surface energy of Cr compared to Mn, Mg and Cu. Working at 210 °C with a low thickness Cr/ITO film they obtained a good linear response in the range of concentration 30–100 ppm of benzene and a good selectivity compared to toluene.

4.8. Other VOC sensors

Compared with above mentioned VOCs, there is a paucity of research works on the development of cyclohexene, 2-propanol and n-butanol sensors (Table 10).

Up to date, only Gao et al. [205,206] proposed a cyclohexene sensor based on metal oxide. They synthesized WO₃ nanoplates by hydrothermal method. The WO₃ sensor showed the best response of 21 (R_a/R_g) to cyclohexene at 1000 ppm as compared with that of 15.1 to acetone and 6.0 to ethanol.

Likewise of the cyclohexene sensors, no many papers report about the use of metal oxides as 2-propanol sensors. Huang et al. [207] synthesized hematite solid spindles and hollow spindles by a template-free, economical hydrothermal method. Compared with other hematite nanostructures, the porous hollow hematite spindles showed better performance in gas sensing due to their large surface area and porous hollow structure. As reported, the α -Fe₂O₃ porous hollow spindle sensor showed high sensitivity to 100 ppm 2-propanol ($R_a/R_g=24$). However this sensor was not selective to 2-propanol because it also responses to acetone in a similar way.

Table 9

List of metal oxide based benzene sensors.

Material	Conc. (ppm)	Response	T (°C)	Res. time/ Rec. time (s)	Refs.
SmFeO ₃	3	9 ^a	400	-/-	[44]
ZnO-TiO ₂	100	27 ^a	370	10/5	[43]
ZnO NR	100	2.5 ^a	300	-/-	[127]
Ce-doped In ₂ O ₃	100	2.5 ^a	320	-/-	[180]
Mesoporous worm-like SnO ₂ NPs	10	20 ^a	150	-/-	[165]
WO ₃ thick film	20	12.5 ^b	200	70/120	[201]
Cu ₂ O octahedral NPs	50	9.7 ^a	230	3/4	[202]
Flower-shaped SnO ₂ NPs	150	3.25 ^a	240	-/-	[203]
Cr/ ITO thin film	1000	72 ^b	210	38/53	[204]

^a (R_a/R_g , %).

^b (R_a/R_g).

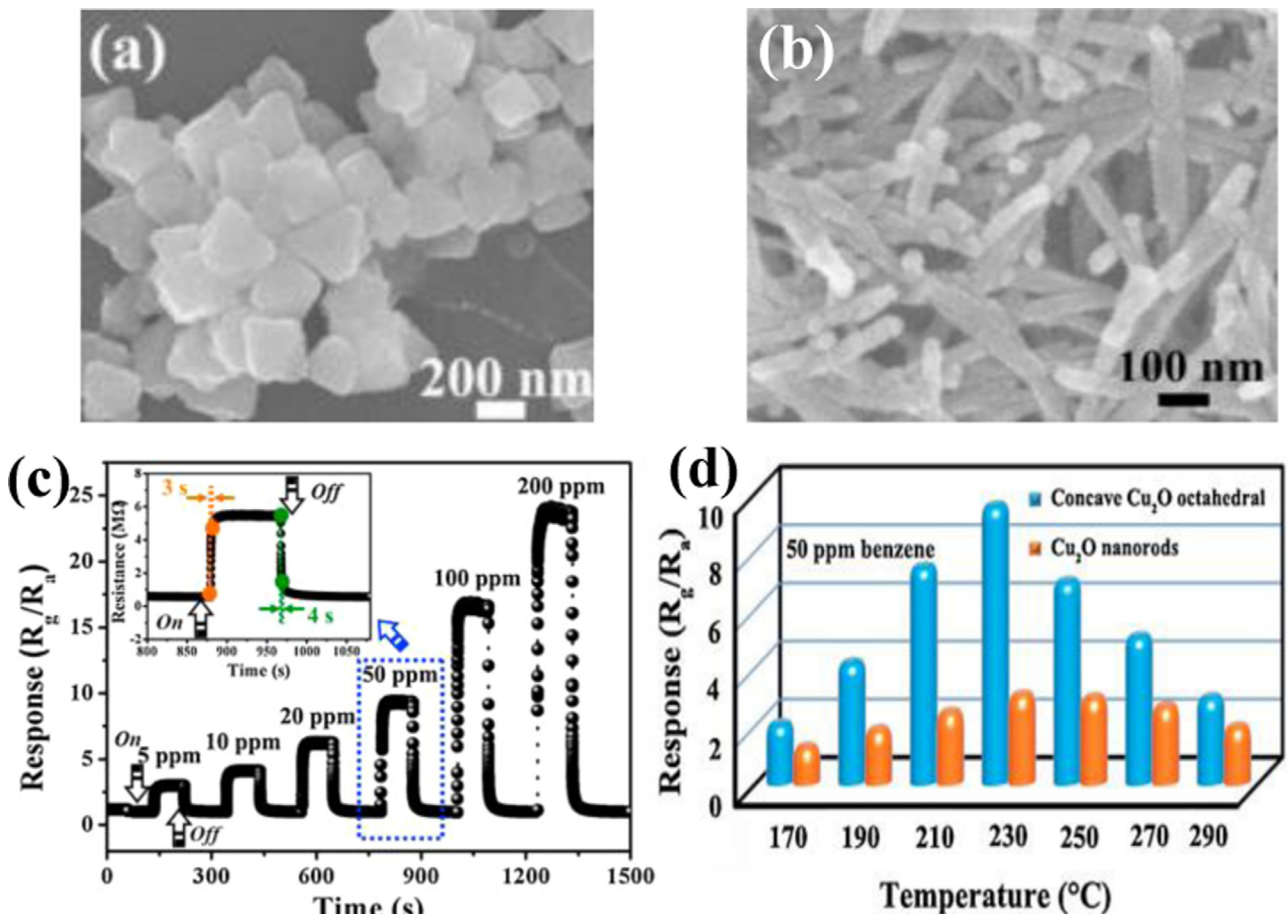


Fig. 19. SEM images of: a) Cu_2O octahedral nanostructures; b) Cu_2O nanorods. c) Dynamic response curve of the sensor based on Cu_2O octahedral nanostructures to benzene with concentrations ranging from 5 to 200 ppm at the operating temperature of 230 °C. d) Gas sensitivities of the Cu_2O octahedral (blue) and Cu_2O nanorods (orange) sensors measured at different operating temperatures to 50 ppm of benzene [202]. (For interpretation of the references to color in this figure legend, the reader is referred to the web version of this article.)

Table 10
List of metal oxide based cyclohexene, 2-propanol and n-butanol sensors.

Material	Conc. (ppm)	Response	T (°C)	Refs.
Cyclohexene				
WO ₃ nanoplates	1000	140 ^a	300	[205]
WO ₃ 0.33H ₂ O nanoplates	1000	21 ^a	370	[206]
2-Propanol				
SmFeO ₃	3	29 ^a	400	[44]
3 wt% PdO doped SnO ₂	N/A	86.3 ^b	350	[133]
3D aloe-like SnO ₂ nanostructures	50	14 ^a	240	[46]
Flower like ZnO NPs	100	14.2 ^a	320	[115]
α -Fe ₂ O ₃ porous hollow spindle	100	14 ^a	280	[207]
n-Butanol				
α -Fe ₂ O ₃ -Au-ZnO	200	134 ^a	225	[135]
ZnO decorated α -Fe ₂ O ₃	200	65 ^a	225	[139]
Mesoporous worm-like SnO ₂ NPs	10	625 ^a	150	[165]
Flower like ZnO NPs	100	24.1 ^a	320	[115]
α -Fe ₂ O ₃ porous hollow spindle	100	14 ^a	280	[207]
Flower-shaped SnO ₂ NPs	100	80 ^a	240	[203]

^a (R_a/R_g).

^b ($(R_a-R_g)/R_a$, %).

Unlike the above last two VOCs, some additional work may be found regarding the use of metal oxides for the detection of n-butanol. Kaneti et al. [135] reported a series α -Fe₂O₃ based materials as an n-butanol sensors. The ternary α -Fe₂O₃-ZnO-Au nanocomposites were found to show higher responses (R_a/R_g) of 113 towards 100 ppm n-butanol compared to single α -Fe₂O₃ and binary α -Fe₂O₃-ZnO sensing materials of 11.7 and 54.4,

respectively, even working at lower operating temperature (225 °C). They attributed the enhanced sensitivity of the ternary nanocomposites to the chemical sensitization effect induced by the Au nanoparticles and the existence of conjugated depletion layers in the nanocomposites which promoted a greater drop in resistance upon exposure to the gas.

Wang et al. [165] synthesized mesoporous worm-like SnO₂ architectures via a simple hydrothermal process. The worm-like SnO₂ nanostructures exhibited highly sensitivity, selectivity and a good linear relationship with n-butanol concentrations varied from 5 ppm to 100 ppm in logarithmic scale.

Huang et al. [115] reported large-scale flowerlike ZnO nanostructure using a very simple solution method at near room temperature. The sensor showed good sensitivity and fast response towards n-butanol. The 3D flowerlike ZnO nanostructure film was suggested to allow fast diffusion of gas molecules, resulting in a high rate of gas adsorption and desorption.

5. Selectivity and effect of humidity

The high sensitivity, fast response/recovery times and low operation temperature are not enough parameters to define a good gas sensor. A most important feature to consider is the selectivity, i.e. the ability of the sensor to discriminate the VOC of interest when this is present together with similar others. The selectivity, sometime also defined as cross sensitivity, can be defined by an interfering ratio as:

$$K = S_A/S_B \quad (5)$$

where S_A and S_B are the responses of a sensor to the target VOC and an interfering VOC, respectively, for equivalent concentrations [208]. When the interfering ratio tends to one, the sensor shows no selectivity because the responses to the different compounds become comparable.

This concept arises from the evidence that a chemical sensor may be sensitive not only to the target specie but also to others that can be present in the ambient. In fact, metal oxide gas sensors are normally sensitive to more than one gaseous/vapor specie and usually show cross sensitivity.

As discussed above, the sensitivity to a specific chemical species depends on the type of interaction that it has with the metal oxide surface. This means that similar molecules have similar interactions with the same metal oxide nanostructure, therefore it will result in sensor responses whenever one of them is present in the measuring environment. For this reason, many metal oxides have been proposed as sensitive materials for generic VOCs detection [42–44,61,132,178]. For example, there have been many studies on various sensor materials for detecting both ethanol and acetone; in fact the sensing behavior to ethanol and acetone are similar in most investigations [209], and cross sensitivity between them cannot be avoided. As an another example toluene is a derivative of benzene, so it is very difficult to obtain a metal oxide sensor with high selectivity to benzene with respect to toluene [204]. However, numerous studies have confirmed that different classes of gases have different reaction rates on different metal oxides. For example, ethanol oxidizes on the metal oxide surfaces at relatively low temperatures, whereas other alcohols and ketones do so at intermediate temperatures (200 °C or above), and alkanes (propane and methane in particular) oxidize at higher temperatures (above 400 °C) [91]. This means that by changing the operating temperature is possible to create the right conditions where the response to one gas will exceed considerably the response to another one [210].

Many efforts are devoted to enhance the selectivity of VOCs conductometric metal oxide sensors. Some of these studies are discussed here in detail. Xing et al. [116] reported the use of In_2O_3/Au nanorods as ethanol and acetone sensor. They demonstrated that optimizing the ratio of In/Au was possible to separate the optimal operation temperature to detect selectively ethanol or acetone. In particular, they found that for a specific composition, it was possible to obtain the optimal operation temperature at 250 and 400 °C for acetone and ethanol respectively. In this way, by changing the operational temperature it was possible to use the

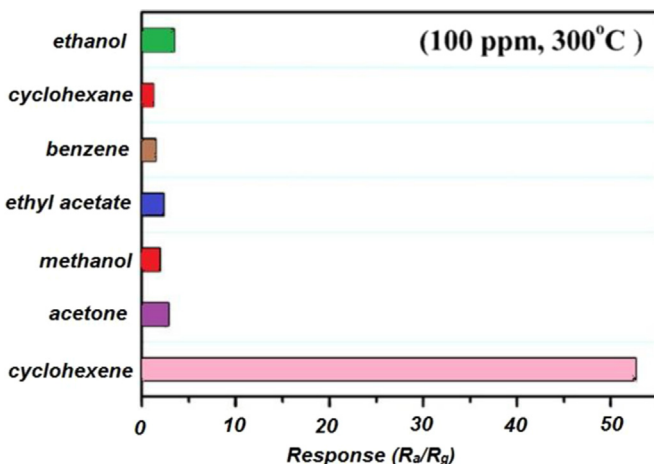


Fig. 20. Responses of the WO_3 nanoplate-based sensor to the 100 ppm of gases tested at 300 °C [205].

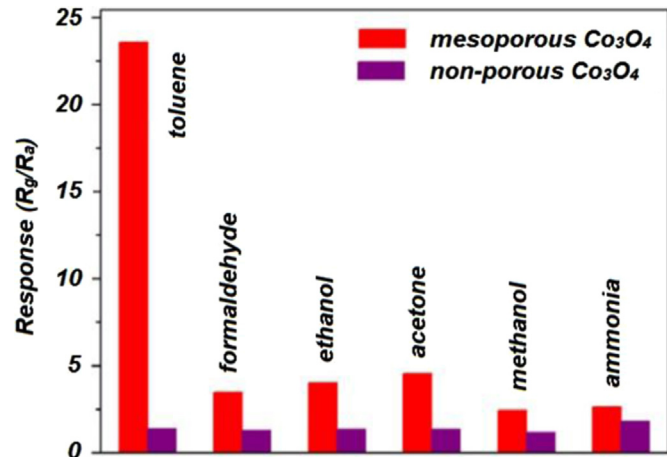


Fig. 21. Selectivity of the sensors based on mesoporous and non-porous Co_3O_4 towards toluene at 190 °C [172].

same sensor for both acetone and ethanol detection.

Gao et al. [205] reported a WO_3 cyclohexene sensor with very high selectivity. Fig. 20 shows the response of the WO_3 nanoplates sensor towards different VOCs at 300 °C. Under the given experimental conditions, the response of the sensor to cyclohexene was approximately 15–25 times higher than that to other gases, indicating the WO_3 nanoplates as a high selective material for cyclohexene detection among the other VOCs examined. The authors attributed the enhanced cyclohexene sensing performance to the thin plate-like morphology and the high crystallinity of the WO_3 nanoplates, which leads to an efficient adsorption and fast diffusion of the cyclohexene molecules. However, they did not justify the selectivity to cyclohexene compared to similar VOCs.

Liu et al. [172] reported highly sensitive and selective toluene sensors based on ordered mesoporous Co_3O_4 . The response of the sensors at 190 °C to 100 ppm toluene was $R_a/R_g=23.55$, while the responses to other gases was about 5 times lower, indicating the high selectivity of the sensors towards toluene sensing. Moreover, the authors, comparing mesoporous with non-porous Co_3O_4 based sensors, showed a remarked selectivity for the mesoporous structures than the other one (Fig. 21). Although the relatively low operating temperature for toluene sensing could be justified by the introduction of a mesoporous structure, the motivation of excellent selectivity obtained has been not clarified.

Tamaekong et al. [194] reported a very high selective acetylene sensor based on 2 at% Pt/ZnO nanoparticles. As it shown in Fig. 22,

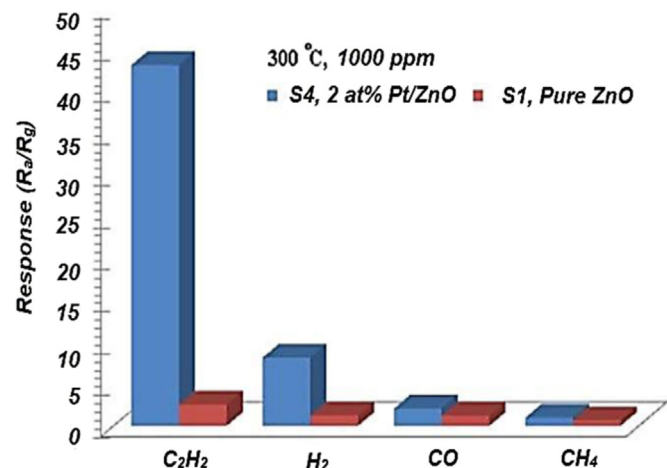


Fig. 22. Selectivity of the sensors based on pure and Pt/ZnO towards acetylene [194].

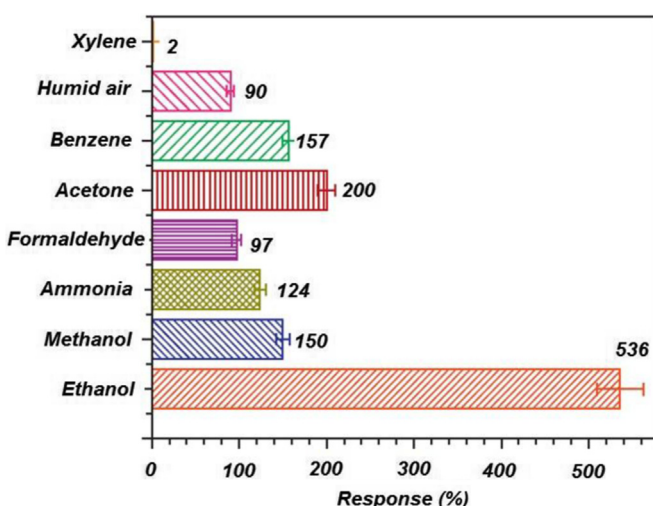


Fig. 23. Sensing response of a TiO_2 thin film towards 50 ppm of ethanol and other VOCs at 30 °C [95].

compared to pure ZnO , the sensor based on Pt-loaded ZnO showed higher selectivity to acetylene respect to other reducing gas as hydrogen, carbon monoxide and methane. This suggests that, in this case, the platinum is responsible for the enhanced selectivity. Although the authors showed a high sensitivity to acetylene compared to a similar hydrocarbon molecule as like methane, no information about the sensitivity to other VOCs has been reported.

Pandeeswari et al. [95] reported a selective ethanol sensor using TiO_2 thin films. The sensing response of sol gel dip-coated TiO_2 thin film towards different reducing vapors such as ethanol, methanol, ammonia, formaldehyde, acetone, benzene, humid air (54% RH) and xylene at a fixed concentration of 50 ppm is shown in Fig. 23. The responses towards some organic vapors investigated were not greater than half of the ethanol response.

Li et al. [211] synthesized $\text{Au}@\text{In}_2\text{O}_3$ and In_2O_3 nanoparticles for formaldehyde detection. As shown in Fig. 24, it is obvious that both sensors exhibited higher response to formaldehyde in comparison to other target gases. Besides, the sensor based on the $\text{Au}@\text{In}_2\text{O}_3$ core-shell microstructures, in comparison to pure In_2O_3 one, showed better sensing performance for each gas and in particular towards formaldehyde. The observed results suggest that

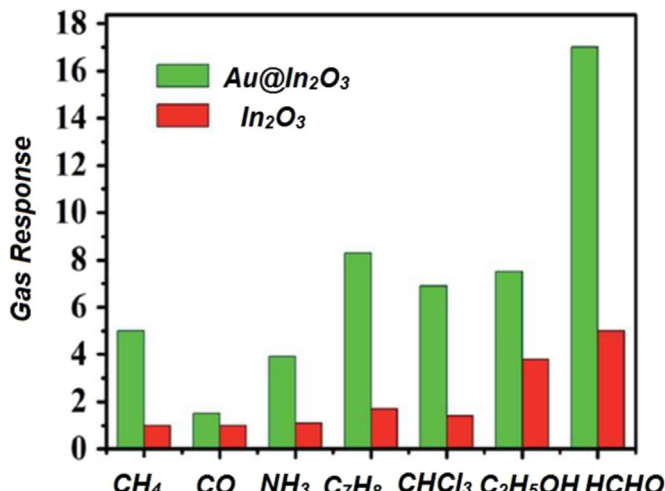


Fig. 24. Response of the sensors based on $\text{Au}@\text{In}_2\text{O}_3$ and In_2O_3 to 100 ppm various gases at 200 °C [211].

Au effect is to promote the selectivity towards this VOC.

According to what above reported, it is clear that the selectivity of metal oxide VOCs sensors can be improved by acting on the features of the sensitive material as well as on the operating parameters of the sensor.

Similar interfering effects derived also from water molecules which are always present in the vast majority of situations due to environmental humidity. Almost all types of metal oxides show a strong tendency to adsorb humidity onto their surfaces. This sorption leads to interfering effects or degradation of the sensing performance. In the first case, the water molecules reacting with chemisorbed oxygen species or directly adsorbing as ionic species, likewise to other gases, lead to a modification of the energy barrier then to the response of the sensor. More commonly, the effect of humidity results in a modification of the metal oxide sensitivity. In fact, the adsorption of water molecules, on the one hand, replace chemisorbed oxygen then reducing the number of active sites, for another hand, humidity make difficult the adsorption then the reactions of the species of interest, in both cases reducing the sensitivity [196]. The humidity is also a cause of long-term performance degradation. Indeed, prolonged exposure of metal oxides to humidity could cause a gradual formation of stable hydroxyl groups on their surface resulting in a progressive decreasing of the sensitivity. However, because this hydroxyl groups start to desorb at temperature higher than 400 °C [41], when it is possible, a proper thermal treatment could restore the initial performance of the metal oxide sensors.

Although the humidity is most of the times an interfering factor for the metal oxide sensors, compensation methods may be used effectively [212]. Furthermore, as extensively previously discussed, many nanostructures have proved able to provide excellent sensitivity and selectivity to the VOCs even in presence of medium-high RH levels [40,116,119,199].

Very interesting work is a study published by de Lacy Costello et al. [213] which tested the response to different VOCs of pure tin oxide, zinc oxide, indium oxide and their binary composition (50:50 w/w) for different humidity ranging from 0 to 100% RH. The study showed that the binary composition of metal oxides gave additional advantage over single oxide sensor as well as increase in sensitivity. In particular, testing alcohols such as ethanol, they observed a reduction in sensitivity working at 100% RH compared to dry condition (Fig. 25), however, the sensor based on binary $\text{SnO}_2/\text{In}_2\text{O}_3$ composite was able to maintain high sensitivity when operated under high humidity conditions. The authors also showed that, in presence of water vapor, although the sensitivity was reduced for alcohols species, it did not affect the response towards carbonyl-containing compounds and non-polar alkanes/aromatics species. This would provide the evidence that different VOCs react with different sites on metal oxide surface.

6. Conclusions and outlook

Conductometric VOCs sensors based on nanostructured metal oxides for detection of ten important VOCs including acetone ($\text{C}_3\text{H}_6\text{O}$), acetylene (C_2H_2), benzene (C_6H_6), cyclohexene (C_6H_{12}), ethanol ($\text{C}_2\text{H}_5\text{OH}$), formaldehyde (HCHO), n-butanol ($\text{C}_4\text{H}_9\text{OH}$), methanol (CH_3OH), toluene (C_7H_8), and 2-propanol ($\text{C}_3\text{H}_8\text{O}$) were reviewed.

From a survey of literature, it can be deduced that ZnO , SnO_2 , WO_3 , In_2O_3 , TiO_2 and $\alpha\text{-Fe}_2\text{O}_3$, showing nanostructured morphologies such as nanoparticles, nanotubes, nanofibers, nanowires, nanorods are the most promising for detection of VOCs with detection limits of few parts per billion. Among the different VOCs, the detection of both ethanol and acetone sensors has been widely

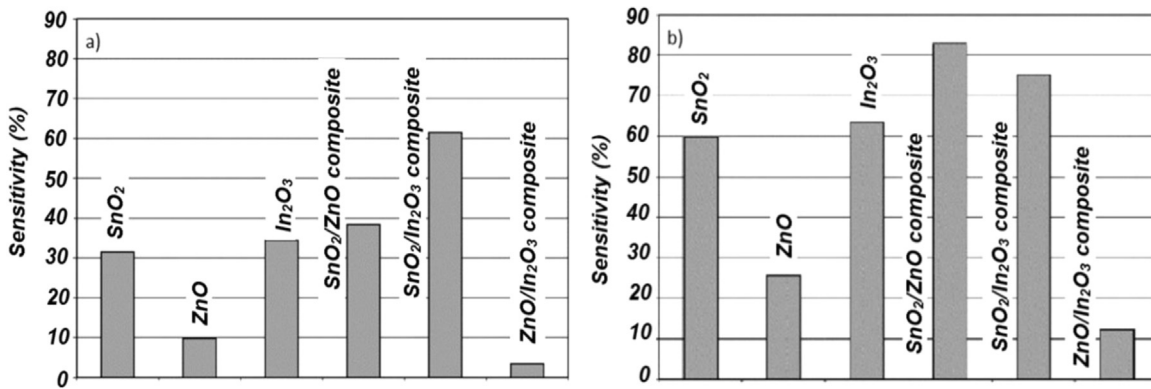


Fig. 25. Responses of single oxide and composites oxides based sensors to 5 ppm of ethanol at: a) 100% RH; b) dry air [213].

studied, whereas very few reports about other important VOCs such as benzene and acetylene can be find in literature. The selectivity remains however a relevant problem of the metal oxide based VOCs gas sensors. Therefore, new metal oxide materials with higher selectivity need to be used for these sensors.

Major efforts will be needed to further engineer such devices. VOCs sensor devices for practical applications must meet stringent requirements for durability, reliability, and energy efficiency. Further investigations must be carried out such as accuracy, calibration, and robustness tests. Based on that, there are a lot of reasons that speak for use of conductometric sensors efficient, reliable and attractive tools for VOCs detection.

Acknowledgements

Partial support of the Iran Nanotechnology Initiative Council, IRAN (Grant No. 12134) is gratefully acknowledged (A.M.).

References

- [1] R. Koppmann, Volatile Organic Compounds in the Atmosphere, Blackwell Publishing Ltd., Oxford, UK, 2007.
- [2] W. Hailin, N. Lie, L. Jing, W. Yufei, W. Gang, W. Junhui, H. Zhengping, Characterization and assessment of volatile organic compounds (VOCs) emissions from typical industries, *Chin. Sci. Bull.* 58 (2013) 724–730.
- [3] A. Tiwary, J. Colls, Air Pollution: Measurement, Modelling and Mitigation, CRC Press, Boca Raton, US, 2009.
- [4] J. Bartzis, P. Wolkoff, M. Stranger, G. Efthimiou, E. Tolis, F. Maes, A. Nørgaard, G. Ventura, K. Kalimeri, E. Goelen, On organic emissions testing from indoor consumer products' use, *J. Hazard. Mater.* 285 (2015) 37–45.
- [5] M. Leidinger, T. Sauerwald, T. Conrad, W. Reimringer, G. Ventura, A. Schütze, Selective detection of hazardous indoor VOCs using metal oxide gas sensors, *Procedia Eng.* 87 (2014) 1449–1452.
- [6] P. Kumar, A. Deep, K.-H. Kim, R.J.C. Brown, Coordination polymers: Opportunities and challenges for monitoring volatile organic compounds, *Prog. Polym. Sci.* 45 (2015) 102–118.
- [7] K. Kawamura, Md Vestergaard, M. Ishiyama, N. Nagatani, T. Hashiba, E. Tamiya, Development of a novel hand-held toluene gas sensor: Possible use in the prevention and control of sick building syndrome, *Measurement* 39 (2006) 490–496.
- [8] L.S.G. Teixeira, E.S. Leão, A.L.F. Dantas, H.S.L.C. Pinheiro, A.C.S. Costa, J.B. de Andrade, Determination of formaldehyde in Brazilian alcohol fuels by flow-injection solid phase spectrophotometry, *Talanta* 64 (2004) 711–715.
- [9] P. Vesely, L. Lusk, G. Basarova, J. Seabrooks, D. Ryder, Analysis of aldehydes in beer using solid-phase microextraction with on-fiber derivatization and Gas Chromatography/Mass Spectrometry, *J. Agric. Food Chem.* 51 (2003) 6941–6944.
- [10] P.J. Sabourin, W.E. Bechtold, R.F. Henderson, A high pressure liquid chromatographic method for the separation and quantitation of water-soluble radiolabeled benzene metabolites, *Anal. Biochem.* 170 (1988) 316–327.
- [11] T.L.W. Zeng, Z. Wang, S. Tsukimoto, M. Saito, Y. Ikuhara, Selective detection of formaldehyde gas using a Cd-doped TiO_2 - SnO_2 Sensor, *Sensors* 9 (2009) 9029.
- [12] V.K. Khanna, Nanosensors Physical, Chemical, and Biological, 1st ed., CRC Press, 2012.
- [13] V. Balouria, A. Kumar, S. Samanta, A. Singh, A.K. Debnath, A. Mahajan, R. Bedi, D.K. Aswal, S.K. Gupta, Nano-crystalline Fe_2O_3 thin films for ppm level detection of H_2S , *Sens. Actuators B: Chem.* 181 (2013) 471–478.
- [14] K.S.N. Yamazoe, New perspectives of gas sensor technology, *Sens. Actuators B* 138 (2009) 100–107.
- [15] R. Jaaniso, O.K. Tan, Semiconductor Gas Sensors, Woodhead Publishing Limited, Cambridge, UK, 2013.
- [16] Z. Zhu, C.-T. Kao, R.-J. Wu, A highly sensitive ethanol sensor based on $\text{Ag}@\text{TiO}_2$ nanoparticles at room temperature, *Appl. Surf. Sci.* 320 (2014) 348–355.
- [17] B.T. Raut, P.R. Godse, S.G. Pawar, M.A. Chougule, D.K. Bandgar, V.B. Patil, Novel method for fabrication of polyaniline-CdS sensor for H_2S gas detection, *Measurement* 45 (2012) 94–100.
- [18] G. Korotcenkov, Metal oxides for solid-state gas sensors: what determines our choice? *Mater. Sci. Eng. B* 139 (2007) 1–23.
- [19] X. Liu, S. Cheng, H. Liu, S. Hu, D. Zhang, H. Ning, A survey on gas sensing technology, *Sensors* 12 (2012) 9635–9665.
- [20] L.B.-T. Hübert, G. Black, U. Banach, Hydrogen sensors – a review, *Sens. Actuators B* 157 (2011) 329–352.
- [21] C. Massie, G. Stewart, G. McGregor, J.R. Gilchrist, Design of a portable optical sensor for methane gas detection, *Sens. Actuators B* 113 (2006) 830–836.
- [22] S. Sharma, M. Madou, A new approach to gas sensing with nanotechnology, *Philos. Trans. R. Soc. A: Math. Phys. Eng. Sci.* 370 (2012) 2448–2473.
- [23] Y.-F. Sun, S.-B. Liu, F.-L. Meng, J.-Y. Liu, Z. Jin, L.-T. Kong, J.-H. Liu, Metal oxide nanostructures and their gas sensing properties: a Review, *Sensors* 12 (2012) 2610–2631.
- [24] J. Zhang, X. Liu, G. Neri, N. Pinna, Nanostructured materials for room-temperature gas sensors, *Adv. Mater.* 28 (2016) 795–831.
- [25] N. Yamazoe, New approaches for improving semiconductor gas sensors, *Sens. Actuators B* 5 (1991) 7–19.
- [26] J.-Q. Ni, W.P. Robarge, C. Xiao, A.J. Heber, Volatile organic compounds at swine facilities: a critical review, *Chemosphere* 89 (2012) 769–788.
- [27] N.A. Downie, Industrial Gases, Kluwer Academic Publishers, New York, US, 2002.
- [28] V.S. Vaishnav, P.D. Patel, N.G. Patel, Indium tin oxide thin film gas sensors for detection of ethanol vapours, *Thin Solid Films* 490 (2005) 94–100.
- [29] P. Patnaik, A Comprehensive Guide to the Hazardous Properties of Chemical Substances, John Wiley & Sons, New Jersey, US, 2007.
- [30] (<http://www.cdc.gov/niosh/dldh/intridl4.html>), 2015.
- [31] O. Bunkoed, F. Davis, P. Kanatharana, P. Thavarungkul, S.P.J. Higson, Sol-gel based sensor for selective formaldehyde determination, *Anal. Chim. Acta* 659 (2010) 251–257.
- [32] A.S.M. Iftekhar Uddin, D.-T. Phan, G.-S. Chung, Low temperature acetylene gas sensor based on Ag nanoparticles-loaded ZnO -reduced graphene oxide hybrid, *Sens. Actuators B* 207 (2015) 362–369.
- [33] J.H.C.S. Lee, Y.H. Park, Development of metal-loaded mixed metal oxides gas sensors for the detection of lethal gases, *J. Ind. Eng. Chem.* 29 (2015) 321–329.
- [34] P.H.M. Mabrook, Benzene sensing using thin films of titanium dioxide operating at room temperature, *Sensors* 2 (2002) 374.
- [35] M.-T. Ke, M.-T. Lee, C.-Y. Lee, L.-M. Fu, A. MEMS-based, benzene gas sensor with a self-heating WO_3 sensing layer, *Sensors* 9 (2009) 2895.
- [36] R.A. Kadir, R.A. Rani, A.S. Zooflakar, J.Z. Ou, M. Shafiei, W. Włodarski, K. Kalantar-zadeh, Nb_2O_5 Schottky based ethanol vapour sensors: effect of metallic catalysts, *Sens. Actuators B: Chem.* 202 (2014) 74–82.
- [37] Z. Zhu, R.-J. Wu, The degradation of formaldehyde using a $\text{Pt}@\text{TiO}_2$ nanoparticles in presence of visible light irradiation at room temperature, *J. Taiwan Inst. Chem. Eng.* 50 (2015) 276–281.
- [38] I. Castro-Hurtado, G.G. Mandayo, E. Castaño, Conductometric formaldehyde gas sensors. A review: from conventional films to nanostructured materials, *Thin Solid Films* 548 (2013) 665–676.
- [39] N.G. Patel, P.D. Patel, V.S. Vaishnav, Indium tin oxide (ITO) thin film gas sensor for detection of methanol at room temperature, *Sens. Actuators B* 96 (2003) 180–189.

- [40] M. Karmaoui, S.G. Leonardi, M. Latino, D.M. Tobaldi, N. Donato, R.C. Pullar, M.P. Seabra, J.A. Labrincha, G. Neri, Pt-decorated In_2O_3 nanoparticles and their ability as a highly sensitive ($< 10 \text{ ppb}$) acetone sensor for biomedical applications, *Sens. Actuators B* 230 (2016) 697–705.
- [41] C. Wang, L. Yin, L. Zhang, D. Xiang, R. Gao, Metal oxide gas sensors: sensitivity and influencing factors, *Sensors* 10 (2010) 2088–2106.
- [42] V. Dobrokhotov, A. Larin, D. Sowell, Vapor trace recognition using a single nonspecific chemiresistor, *Sensors* 13 (2013) 9016–9028.
- [43] B.L. Zhu, C.S. Xie, W.Y. Wang, K.J. Huang, J.H. Hu, Improvement in gas sensitivity of ZnO thick film to volatile organic compounds (VOCs) by adding TiO_2 , *Mater. Lett.* 58 (2004) 624–629.
- [44] M. Mori, Y. Itagaki, J. Iseda, Y. Sadaoka, T. Ueda, H. Mitsuhashi, M. Nakatani, Influence of VOC structures on sensing property of SmFeO_3 semiconductive gas sensor, *Sens. Actuators B* 202 (2014) 873–877.
- [45] K.J.A. Mirzaei, B. Hashemi, A. Bonavita, M. Bonyani, G.N.S. G.Leonardi, Synthesis, characterization and gas sensing properties of $\text{Ag}@\alpha\text{-Fe}_2\text{O}_3$ core-shell nanocomposites, *Nanomaterials* 5 (2015) 737.
- [46] L. Mei, J. Deng, X. Yin, M. Zhang, Q. Li, E. Zhang, Z. Xu, L. Chen, T. Wang, Ultrasensitive ethanol sensor based on 3D aloe-like SnO_2 , *Sens. Actuators B* 166–167 (2012) 7–11.
- [47] Z. Lou, J. Deng, L. Wang, L. Wang, T. Fei, T. Zhang, Toluene and ethanol sensing performances of pristine and PdO -decorated flower-like ZnO structures, *Sens. Actuators B* 176 (2013) 323–329.
- [48] J.Y.P.L.K. Bagal, M.V. Vaishampayan, I.S. Mulla, S.S. Suryavanshi, Effect of Pd and Ce on the enhancement of ethanol vapor response of SnO_2 thick films, *Sens. Actuators B* 207 (2015) 383–390.
- [49] C. Balamurugan, A.R. Maheswari, D.W. Lee, Structural, optical, and selective ethanol sensing properties of p-type semiconducting CoNb_2O_6 nanopowder, *Sens. Actuators B* 205 (2014) 289–297.
- [50] X.W.J. Liu, Q. Peng, Y. Li, Vanadium pentoxide nanobelts: highly selective and stable ethanol sensor materials, *Adv. Mater.* 17 (2005) 764–767.
- [51] Y. Wang, Y. Lin, D. Jiang, F. Li, C. Li, L. Zhu, S. Wen, S. Ruan, Special nanostructure control of ethanol sensing characteristics based on $\text{Au}@\text{In}_2\text{O}_3$ sensor with good selectivity and rapid response, *RSC Adv.* 5 (2015) 9884–9890.
- [52] X. Xu, H. Fan, Y. Liu, L. Wang, T. Zhang, Au-loaded In_2O_3 nanofibers-based ethanol micro gas sensor with low power consumption, *Sens. Actuators B* 160 (2011) 713–719.
- [53] P. Song, D. Han, H. Zhang, J. Li, Z. Yang, Q. Wang, Hydrothermal synthesis of porous In_2O_3 nanospheres with superior ethanol sensing properties, *Sens. Actuators B* 196 (2014) 434–439.
- [54] V.N. Singh, B.R. Mehta, R.K. Joshi, F.E. Kruis, S.M. Shivaprasad, Enhanced gas sensing properties of In_2O_3 : Ag composite nanoparticle layers; electronic interaction, size and surface induced effects, *Sens. Actuators B* 125 (2007) 482–488.
- [55] Z. Li, Y. Dzenis, Highly efficient rapid ethanol sensing based on Co-doped In_2O_3 nanowires, *Talanta* 85 (2011) 82–85.
- [56] A.S.M.A.H.T. Tharsika, Sheikh A. Akbar, Mohd Faizul Mohd Sabri, Wong Yew Hoong, Enhanced ethanol gas sensing properties of SnO_2 -Core/ ZnO -Shell Nanostructures, *Sensors* 14 (2014) 14586–14600.
- [57] R.-J. Wu, D.-J. Lin, M.-R. Yu, M.H. Chen, H.-F. Lai, Ag@ SnO_2 core-shell material for use in fast-response ethanol sensor at room operating temperature, *Sens. Actuators B* 178 (2013) 185–191.
- [58] Y.-J. Chen, C.-L. Zhu, G. Xiao, Ethanol sensing characteristics of ambient temperature sonochemically synthesized ZnO nanotubes, *Sens. Actuators B* 129 (2008) 639–642.
- [59] C.T.K.Z. Zhu, R.J. Wu, A highly sensitive ethanol sensor based on $\text{Ag}@\text{TiO}_2$ nanoparticles at room temperature, *Appl. Surf. Sci.* 320 (2014) 348–355.
- [60] H.K.S. Park, S. An, W. Lee, S. Lee, C. Lee, Synthesis and ethanol sensing properties of CuO nanorods coated with In_2O_3 , *Ceram. Int.* 39 (2013) 5255–5262.
- [61] E.S.N. Kilinc, Z.Z. Ozturk, Fabrication of TiO_2 nanotubes by anodization of Ti thin films for VOC sensing, *Thin Solid Films* 520 (2011) 953–958.
- [62] X.Y. Xue, Y.J. Chen, Y.G. Wang, T.H. Wang, Synthesis and ethanol sensing characteristics of single crystalline SnO_2 nanorods, *Appl. Phys. Lett.* 87 (2005) 233503–233505.
- [63] Y.M.F. Pourfayaz, A. Khodadadi, S. Ajami, Ceria-doped SnO_2 sensor highly selective to ethanol in humid air, *Sens. Actuators B* 130 (2008) 625–629.
- [64] C.L. Hsu, T.J. Hsueh, S.J. Chang, I.C. Chen, Laterally grown ZnO nanowire ethanol gas sensors, *Sens. Actuators B* 126 (2007) 473–477.
- [65] G. Du, P. Hu, W. Zhou, J. Cui, J. Lin, H. Liu, D. Liu, J. Wang, S. Chen, Enhancement of ethanol vapor sensing of TiO_2 nanobelts by surface engineering, *Appl. Mater. Interfaces* 2 (2010) 3263–3269.
- [66] D.J.X. Chu, Y. Guo, C. Zheng, Ethanol gas sensor based on CoFe_2O_4 nanocrystallines prepared by hydrothermal method, *Sens. Actuators B* 120 (2006) 177–181.
- [67] K.M. Li, Y.J. Li, C.Y. Wang, C.I. Kuo, L.J. Chen, Low-temperature electro-deposited Co-doped ZnO nanorods with enhanced ethanol and CO sensing properties, *Sens. Actuators B* (2012) 734–739.
- [68] W.C.C. Xiangfeng, J. Dongli, Z. Chenmou, Ethanol sensor based on indium oxide nanowires prepared by carbothermal reduction reaction, *Chem. Phys. Lett.* 399 (2004) 461–464.
- [69] D.Z.K. Ryu, C. Zhou High-performance metaloxide, nanowire chemical sensors with integrated micromachined hotplates, *Appl. Phys. Lett.* 92 (2008).
- [70] W.D. Zhang, W.H. Zhang, L.Y. Chen, Highly sensitive detection of explosive tri acetone triperoxide by an In_2O_3 sensor, *Nanotechnology* 21 (2010) 315505.
- [71] Y.C.J. Xu, J. Shen, Ethanol sensor based on hexagonal indium oxide nanorods prepared by solvothermal methods, *Mater. Lett.* 62 (2008) 1363–1365.
- [72] X.L.W. Zheng, W. Wang, Z. Li, H. Zhang, Y. Wang, Z. Wang, C. Wang, A highly sensitive and fast-responding sensor based on electrospun In_2O_3 nanofibers, *Sens. Actuators B* 142 (2009) 61–65.
- [73] S. Wei Jin, Li An, Wen Chen, Shuang Yang, Chunxia Zhao, Ying Dai, Enhancement of ethanol gas sensing response based on ordered V_2O_5 nanowire microyarns, *Sens. Actuators B* 206 (2015) 284–290.
- [74] J. Liu, X. Wang, Q. Peng, Y. Li, Preparation and gas sensing properties of vanadium oxide nanobelts coated with semiconductor oxides, *Sens. Actuators B* 115 (2006) 481–487.
- [75] H. Ko, S. Park, S. An, C. Lee, Enhanced ethanol sensing properties of $\text{TeO}_2/\text{In}_2\text{O}_3$ core-shell nanorod sensors, *Curr. Appl. Phys.* 13 (2013) 919–924.
- [76] N. Rajesh, J.C. Kannan, T. Krishnakumar, S.G. Leonardi, G. Neri, Sensing behavior to ethanol of tin oxide nanoparticles prepared by microwave synthesis with different irradiation time, *Sens. Actuators B* 194 (2014) 96–104.
- [77] B. Mondal, K. Mukherjee, P. Das, Facile synthesis of pseudo-peanut shaped hematite iron oxide nano-particles and their promising ethanol and formaldehyde sensing characteristics, *RSC Adv.* 4 (2014) 31879–31886.
- [78] N. Van Hieu, N.A.P. Duc, T. Trung, M.A. Tuan, N.D. Chien, Gas-sensing properties of tin oxide doped with metal oxides and carbon nanotubes: a competitive sensor for ethanol and liquid petroleum gas, *Sens. Actuators B* 144 (2010) 450–456.
- [79] O.K. Tan, W. Cao, W. Zhu, J.W. Chai, J.S. Pan, Ethanol sensors based on nanosized $\alpha\text{-Fe}_2\text{O}_3$ with SnO_2 , ZrO_2 , TiO_2 solid solutions, *Sens. Actuators B* 93 (2003) 396–401.
- [80] Y.-B. Zhang, J. Yin, L. Li, L.-X. Zhang, L.-J. Bie, Enhanced ethanol gas-sensing properties of flower-like p-CuO/n-ZnO heterojunction nanorods, *Sens. Actuators B* 202 (2014) 500–507.
- [81] H. Zhao, X.L. Cheng, L.H. Huo, S. Gao, J.G. Zhao, ZnO nanoparticulate thin film: preparation,characterization and gas-sensing property, *Sens. Actuator B: Chem.* 102 (2004) 248–252.
- [82] J.H.P. H.Ahn, S.B. Kim, S.H. Jee, Y.S. Yoon, D.J. Kim, Vertically aligned ZnO nanorod sensor on flexible substrate for ethanol gas monitorin, *Electrochem. Solid State Lett.* 13 (2011) J125–J128.
- [83] Y.C.J. Xu, Y. Li, J. Shen, Gas sensing properties of ZnO nanorods prepared by hydrothermal method, *J. Mater. Sci.* 40 (2005) 2919–2921.
- [84] F.G. Bao, L. Wang, Y. Wang, Y. Chen, G. Chen, G. Li, C. Chang, W. Qin, Nanorod arrays and hollow spheres through a facile room-temperaturesolution route and their enhanced ethanol gas-sensing properties, *Chem. Plus Chem.* 78 (2013) 1266–1272.
- [85] Y. Chen, C.L. Zhu, G. Xiao, Reduced-temperature ethanol sensing characteristics of flower-like ZnO nanorods synthesized by a sonochemical method, *Nanotechnology* 17 (2006) 4537.
- [86] Q.W.P. Feng, T.H. Wang, Contact-controlled sensing properties of flower like ZnO nanostructures, *Appl. Phys. Lett.* 87 (2005) 213111–213113.
- [87] Y.J.D. J.R.Huang, C.P. Gu, Y.F. Sun, J.H. Liu, Preparationofporousflower-like CuO/ZnO nanostructures and analysis of their gas-sensing property, *J. Alloy. Compd.* 575 (2013) 115–122.
- [88] J.L.J. Zhang, Q. Peng, X. Wang, Y. Li, Nearly monodisperse Cu_2O and CuO nanospheres: preparation and applications for sensitive gas sensors, *Chem. Mater.* 18 (2006) 867–871.
- [89] A.S. Zooflakar, M.Z. Ahmad, R.A. Rani, J.Z. Ou, S. Balendiran, S. Zhuiykov, K. Latham, W. Włodarski, K. Kalantar-zadeh, Nanostructured copper oxides as ethanol vapour sensors, *Sens. Actuators B* 185 (2013) 620–627.
- [90] E.C.D. Barreca, A. Gasparotto, C. Maccato, C. Sada, G. Sberveglieri, E. Tondello, Chemical vapor deposition of copper oxide films and entangled quasi-1D nanoarchitectures as innovative gas sensors, *Sens. Actuators B* 141 (2009) 270–275.
- [91] X.Q.F.C. Wang, X.Y. Xue, Y.G. Wang, T.H. Wang, Surface accumulation conduction controlled sensing characteristic of p-type CuO nanorods induced by oxygen adsorption, *Nanotechnology* 18 (2007).
- [92] A.G.P. Raksa, T. Chairuangsri, P. Mangkorntong, N. Mangkorntong, S. Choopun, Ethanol sensing properties of CuO nanowires prepared by an oxidation reaction, *Ceram. Int.* 35 (2009) 649–652.
- [93] N.D. Khoaing, N. Van Duy, N.D. Hoa, N. Van Hieu, Design of SnO_2/ZnO hierarchical nanostructures for enhanced ethanol gas-sensing performance, *Sens. Actuators B* 174 (2012) 594–601.
- [94] D.T. Thanh Le, D.D. Trung, N.D. Chinh, B.T. Thanh Binh, H.S. Hong, N. Van Duy, N.D. Hoa, N. Van Hieu, Facile synthesis of SnO_2 - ZnO core-shell nanowires for enhanced ethanol-sensing performance, *Curr. Appl. Phys.* 13 (2013) 1637–1642.
- [95] R.K.K.R. Pandeeswari, B.G. Jeyaprakash, Ethanol sensing behaviour of sol-gel dip-coated TiO_2 thin films, *Sens. Actuators B* 194 (2014) 470–477.
- [96] M.X. Shunqiang Liu, Yanxing Li, Xuefeng Guoa, Weijie Ji, Weiping Dinga, Chaktong Au, Novel sea urchin-like hollow core-shell SnO_2 superstructures: Facile synthesis and excellent ethanol sensing performance, *Sens. Actuators B* 151 (2010) 229–235.
- [97] Z. Xu, X. Liu, Y. Liu, Y. Shen, A novel high performance ethanol gas sensor based on $\text{CdO}-\text{Fe}_2\text{O}_3$ semiconducting materials, *Sens. Actuators B* 52 (1998) 270–273.
- [98] A. Bonavita, G. Neri, G. Micali, N. Donato, F.A. Deorsola, P. Mossino, I. Amato, B. De Benedetti, Ethanol sensors based on Pt-doped tin oxide nanopowders

- synthesised by gel-combustion, *Sens. Actuators B* 117 (2006) 196–204.
- [99] Y.J.C.C.L. Zhu, R.X. Wang, L.J. Wang, M.S. Cao, X.L. Shi, Synthesis and enhanced ethanol sensing properties of α -Fe₂O₃/ZnO hetero nanostructures, *Sens. Actuators B* 140 (2009) 185–189.
- [100] H.K. Sujatha Singh, V.N. Singh, Kiran Jain, T.D. Senguttuvan, Highly sensitive and pulse-like response toward ethanol of Nb doped TiO₂ nanorods based gas sensors, *Sens. Actuators B* 171–172 (2012) 899–906.
- [101] G.B.C. Balamurugan, A. Subramania, Development of nanocrystalline CrNbO₄ based p-type semiconducting gas sensor for LPG, ethanol and ammonia, *Sens. Actuators B* 168 (2012) 165–171.
- [102] X.-N.Y. Li-Jian Bie, Jing Yin, Yue-Qin Duan, Zhi-Hao Yuan, Nanopillar ZnO gas sensor for hydrogen and ethanol, *Sens. Actuators B* 126 (2007) 604–608.
- [103] M.Z. Ahmad, A.Z. Sadek, K. Latham, J. Kita, R. Moos, W. Wlodarski, Chemically synthesized one-dimensional zinc oxide nanorods for ethanol sensing, *Sens. Actuators B* 187 (2013) 295–300.
- [104] M.K. Nirajan, S. Ramgir, Preetam K. Sharma, Niyanta Datta, S. Kailasaganapathi, S. Bhattacharya, A.K. Debnath, D.K. Aswal, S.K. Gupta, Ethanol sensing properties of pure and Au modified ZnO nanowires, *Sens. Actuators B* 187 (2013) 313–318.
- [105] Y.Y.L. Zhang, Large-scale synthesis of flower-like ZnO nanorods via a wet-chemical route and the defect-enhanced ethanol-sensing properties, *Sens. Actuators B* 183 (2013) 110–116.
- [106] Y.K.L. Wang, X. Liu, S. Zhang, W. Huang, S. Wang, ZnO nanorod gas sensor for ethanol detection, *Sens. Actuators B* 162 (2012) 237–243.
- [107] Q.H.L.Q. Wan, Y.J. Chen, T.H. Wang, X.L. He, J.P. Li, C.L. Lin, Fabrication and ethanol sensing characteristics of ZnO nanowire gas sensors, *Appl. Phys. Lett.* 82 (2004) 3654–3656.
- [108] N.H.S. Choopun, P. Mangkorntong, N. Mangkorntong, Zinc oxide nanobelts by RF sputtering for ethanol sensor, *Physica E* 39 (2007) 53–56.
- [109] S.J.C.T.J. Hsueh, C.L. Hsu, Y.R. Lin, I.C. Chen, ZnO nanotube ethanol gas sensors, *J. Electrochem. Soc.* 155 (2008) K152–K155.
- [110] R.C.S. Onkar Singh, Enhancement in ethanol sensing response by surface activation of ZnO with SnO₂, *Mater. Res. Bull.* 47 (2012) 557–561.
- [111] H.K. Youngjae Kwon, Sangmin Lee, In-Joo Chind, Tae-Yeon Seonge, Wan In Lee, Chongmu Lee, Enhanced ethanol sensing properties of TiO₂ nanotube sensors, *Sens. Actuators B* 173 (2012) 441–446.
- [112] A.T.S. Choopun, T. Santhaveesuk, S. Nilphai, E. Wongrat, N. Hongsith, Zinc oxide nanostructures for applications as ethanol sensors and dye-sensitized solar cells, *Appl. Surf. Sci.* 256 (2009) 998–1002.
- [113] D.W.T. Santhaveesuk, S. Choopun, Enhancement of sensor response by TiO₂ mixing and Au coating on ZnO tetrapod sensor, *Sens. Actuators B* (2010) 502–507.
- [114] S.W.J. Zhang, X. Liu, B. Cao, S. Zheng, One-pot synthesis of Au-supported ZnO nanoplates with enhanced gas sensor performance, *Sens. Actuators B* 169 (2012) 61–66.
- [115] Y.W.J. Huang, C. Gu, M. Zhai, K. Yu, M. Yang, J. Liu, Large-scale synthesis of flowerlike ZnO nanostructure by a simple chemical solution route and its gas-sensing property, *Sens. Actuators B* (2010) 206–212.
- [116] R. Xing, L. Xu, J. Song, C. Zhou, Q. Li, D. Liu, H.W. Song, Preparation and gas sensing properties of In₂O₃/Au nanorods for detection of volatile organic compounds in exhaled breath, *Sci. Rep.* 5 (2015).
- [117] S.G. Leonardi, A. Mirzaei, A. Bonavita, S. Santangelo, P. Frontera, F. Pantò, P. L. Antonucci, G. Neri, A comparison of the ethanol sensing properties of α -iron oxide nanostructures prepared via the sol-gel and electrospinning techniques, *Nanotechnology* 27 (2016) 075502.
- [118] A. Mirzaei, K. Janghorban, B. Hashemi, G. Neri, Metal-core@ metal oxide-shell nanomaterials for gas-sensing applications: a review, *J. Nanopart. Res.* 17 (2015) 1–36.
- [119] M. Righetto, A. Tricoli, S.E. Pratsinis, Si: WO₃ sensors for highly selective detection of acetone for easy diagnosis of diabetes by breath analysis, *Anal. Chem.* 82 (2010) 3581–3587.
- [120] S. Kim, S. Park, S. Park, C. Lee, Acetone sensing of Au and Pd-decorated WO₃ nanorod sensors, *Sens. Actuators B* 209 (2015) 180–185.
- [121] P. Song, Q. Wang, Z. Yang, Preparation, characterization and acetone sensing properties of Ce-doped SnO₂ hollow spheres, *Sens. Actuators B* 173 (2012) 839–846.
- [122] C. Liu, H. Shan, L. Liu, S. Li, H. Li, High sensing properties of Ce-doped α -Fe₂O₃ nanotubes to acetone, *Ceram. Int.* 40 (2014) 2395–2399.
- [123] R.C. Biswal, Pure and Pt-loaded gamma iron oxide as sensor for detection of sub ppm level of acetone, *Sens. Actuators B* 157 (2011) 183–188.
- [124] H. Shan, C. Liu, L. Liu, S. Li, L. Wang, X. Zhang, X. Bo, X. Chi, Highly sensitive acetone sensors based on La-doped α -Fe₂O₃ nanotubes, *Sens. Actuators B* 184 (2013) 243–247.
- [125] M.S. Khandekar, N.L. Tarwal, I.S. Mulla, S.S. Suryavanshi, Nanocrystalline Ce doped CoFe₂O₄ as an acetone gas sensor, *Ceram. Int.* 40 (2014) 447–452.
- [126] S.F. Bamsaoud, S.B. Rane, R.N. Karekar, R.C. Aiyer, Nano particulate SnO₂ based resistive films as a hydrogen and acetone vapour sensor, *Sens. Actuators B* 153 (2011) 382–391.
- [127] Y. Zeng, T. Zhang, M. Yuan, M. Kang, G. Lu, R. Wang, H. Fan, Y. He, H. Yang, Growth and selective acetone detection based on ZnO nanorod arrays, *Sens. Actuators B* 143 (2009) 93–98.
- [128] X. Li, Y. Chang, Y. Long, Influence of Sn doping on ZnO sensing properties for ethanol and acetone, *Mater. Sci. Eng.: C* 32 (2012) 817–821.
- [129] P. Sun, X. Zhou, C. Wang, K. Shimanoe, G. Lu, N. Yamazoe, Hollow SnO₂/[small alpha]-Fe₂O₃ spheres with a double-shell structure for gas sensors, *J. Mater. Chem. A* 2 (2014) 1302–1308.
- [130] X.-X. Zou, G.-D. Li, P.-P. Wang, J. Su, J. Zhao, L.-J. Zhou, Y.-N. Wang, J.-S. Chen, A precursor route to single-crystalline WO₃ nanoplates with an uneven surface and enhanced sensing properties, *Dalton Trans.* 41 (2012) 9773–9780.
- [131] A. Vomiero, S. Bianchi, E. Comini, G. Faglia, M. Ferroni, N. Poli, G. Sberveglieri, In₂O₃ nanowires for gas sensors: morphology and sensing characterisation, *Thin Solid Films* 515 (2007) 8356–8359.
- [132] K. Inyawilert, A. Wisitsora-at, A. Tuantranont, P. Singhai, S. Phanichphant, C. Liewhiran, Ultra-rapid VOCs sensors based on sparked-In₂O₃ sensing films, *Sens. Actuators B* 192 (2014) 745–754.
- [133] P.P.J.K. Srivastava, V.N. Mishra, R. Dwivedi, Structural and micro structural studies of PbO-doped SnO₂ sensor for detection of methanol, propanol and acetone, *J. Nat. Gas. Chem.* 20 (2011) 179–183.
- [134] A.V. Rajgure, J.Y. Patil, R.C. Pawar, C.S. Lee, S.S. Suryavanshi, Aqueous chemical route deposition of nanocrystalline ZnO thin films as acetone sensor: effect of molarity, *Ceram. Int.* 39 (2013) 87–92.
- [135] J.M. Y.V. Kaneti, M. Liu, Y. Yuan, Q. Zakaria, X. Jiang, A. Yu, Hydrothermal synthesis of ternary α -Fe₂O₃–ZnO–Au nanocomposites with high gas-sensing performance, *Sens. Actuators B* 209 (2015) 889–897.
- [136] X.L.J. Zhang, L. Wang, T. Yang, X. Guo, S. Wu, S. Wang, S. Zhang, Synthesis and gas sensing properties of α -Fe₂O₃/ZnO core–shell nanospindles, *Nano-technology* 22 (2011) 185501.
- [137] F.R.S. Zhang, W. Wu, J. Zhou, X. Xiao, L. Sun, Y. Liu, C. Jiang, Controllable synthesis of recyclable core–shell α -Fe₂O₃@SnO₂ hollow nanoparticles with enhanced photocatalytic and gas sensing properties, *Phys. Chem. Chem. Phys.* 15 (2013) 8228–8236.
- [138] L.M.P. Gunawan, J. Teo, J. Ma, J. Highfield, Q. Li, Z. Zhong, Ultrahigh sensitivity of Au/1D α -Fe₂O₃ to acetone and the sensing mechanism, *Langmuir* 28 (2012) 14090–14099.
- [139] Q.M.D.Z.Y.V. Kaneti, Z. Zhang, C. Chen, J. Yue, M. Liu, X. Jiang, A. Yu, Solvothermal synthesis of ZnO-decorated α -Fe₂O₃ nanorods with highly enhanced gas-sensing performance toward *n*-butanol, *J. Mater. Chem. A* 2 (2014) 13283–13292.
- [140] X.L.J. Zhang, L. Wang, T. Yang, X. Guo, S. Wu, S. Wang, S. Zhang, Au-functionalized hematite hybrid nanospindles: general synthesis, gas sensing and catalytic properties, *J. Phys. Chem. C* 115 (2011) 5352–5357.
- [141] J.Z.X. Liu, X. Guo, S. Wang, S. Wu, Core-shell α -Fe₂O₃@SnO₂/Au hybrid structures and their enhanced gas sensing properties, *RSC Adv.* 2 (2012) 1650–1655.
- [142] P.-R. Chung, C.-T. Tseng, M.-T. Ke, C.-Y. Lee, Formaldehyde gas sensors: a review, *Sensors* 13 (2013) 4468–4484.
- [143] K. Huang, L. Kong, F. Yuan, C. Xie, In situ diffuse reflectance infrared Fourier transform spectroscopy study of formaldehyde adsorption and reactions on nano γ -Fe₂O₃ films, *Appl. Surf. Sci.* 270 (2013) 405–410.
- [144] J. Wang, L. Liu, S.-Y. Cong, J.-Q. Qi, B.-K. Xu, An enrichment method to detect low concentration formaldehyde, *Sens. Actuators B* 134 (2008) 1010–1015.
- [145] H. Zhang, P. Song, D. Han, Q. Wang, Synthesis and formaldehyde sensing performance of LaFeO₃ hollow nanospheres, *Physica E: Low-Dimens. Syst. Nanostruct.* 63 (2014) 21–26.
- [146] F.-C. Chung, R.-J. Wu, F.-C. Cheng, Fabrication of a Au@SnO₂ core–shell structure for gaseous formaldehyde sensing at room temperature, *Sens. Actuators B* 190 (2014) 1–7.
- [147] X. Chu, T. Chen, W. Zhang, B. Zheng, H. Shui, Investigation on formaldehyde gas sensor with ZnO thick film prepared through microwave heating method, *Sens. Actuators B* 142 (2009) 49–54.
- [148] N. Han, X. Wu, D. Zhang, G. Shen, H. Liu, Y. Chen, CdO activated Sn-doped ZnO for highly sensitive, selective and stable formaldehyde sensor, *Sens. Actuators B* 152 (2011) 324–329.
- [149] T. Chen, Q.J. Liu, Z.L. Zhou, Y.D. Wang, The fabrication and gas-sensing characteristics of the formaldehyde gas sensors with high sensitivity, *Sens. Actuators B* 131 (2008) 301–305.
- [150] W. Zeng, T. Liu, Z. Wang, S. Tsukimoto, M. Saito, Y. Ikuhara, Selective detection of formaldehyde gas using a Cd-doped TiO₂-SnO₂ sensor, *Sensors* 9 (2009) 9029.
- [151] C. Xie, L. Xiao, M. Hu, Z. Bai, X. Xia, D. Zeng, Fabrication and formaldehyde gas-sensing property of ZnO–MnO₂ coplanar gas sensor arrays, *Sens. Actuators B* 145 (2010) 457–463.
- [152] J. Wang, P. Zhang, J.-Q. Qi, P.-J. Yao, Silicon-based micro-gas sensors for detecting formaldehyde, *Sens. Actuators B* 136 (2009) 399–404.
- [153] P. Lv, Z.A. Tang, J. Yu, F.T. Zhang, G.F. Wei, Z.X. Huang, Y. Hu, Study on a micro-gas sensor with SnO₂–NiO sensitive film for indoor formaldehyde detection, *Sens. Actuators B* 132 (2008) 74–80.
- [154] L. Peng, J. Zhai, D. Wang, Y. Zhang, P. Wang, Q. Zhao, T. Xie, Size- and photoelectric characteristics-dependent formaldehyde sensitivity of ZnO irradiated with UV light, *Sens. Actuators B* 148 (2010) 66–73.
- [155] N. Han, Y. Tian, X. Wu, Y. Chen, Improving humidity selectivity in formaldehyde gas sensing by a two-sensor array made of Ga-doped ZnO, *Sens. Actuators B* 138 (2009) 228–235.
- [156] C.-Y. Lee, C.-M. Chiang, Y.-H. Wang, R.-H. Ma, A self-heating gas sensor with integrated NiO thin-film for formaldehyde detection, *Sens. Actuators B: Chem.* 122 (2007) 503–510.
- [157] I. Castro-Hurtado, J. Herrán, G.G. Mandayo, E. Castaño, Studies of influence of structural properties and thickness of NiO thin films on formaldehyde detection, *Thin Solid Films* 520 (2011) 947–952.
- [158] I. Castro-Hurtado, J. Herrán, G.G. Mandayo, E. Castaño, SnO₂-nanowires grown by catalytic oxidation of tin sputtered thin films for formaldehyde

- detection, *Thin Solid Films* 520 (2012) 4792–4796.
- [159] F.-C. Chung, Z. Zhu, P.-Y. Luo, R.-J. Wu, W. Li, Au@ZnO core-shell structure for gaseous formaldehyde sensing at room temperature, *Sens. Actuators B* 199 (2014) 314–319.
- [160] G. Zhang, S. Zhang, L. Yang, Z. Zou, D. Zeng, C. Xie, La₂O₃-sensitized SnO₂ nanocrystalline porous film gas sensors and sensing mechanism toward formaldehyde, *Sens. Actuators B* 188 (2013) 137–146.
- [161] Y.M. Zhang, Y.T. Lin, J.L. Chen, J. Zhang, Z.Q. Zhu, Q.J. Liu, A high sensitivity gas sensor for formaldehyde based on silver doped lanthanum ferrite, *Sens. Actuators B* 190 (2014) 171–176.
- [162] H. Du, J. Wang, M. Su, P. Yao, Y. Zheng, N. Yu, Formaldehyde gas sensor based on SnO₂/In₂O₃ hetero-nanofibers by a modified double jets electrospinning process, *Sens. Actuators B* 166–167 (2012) 746–752.
- [163] J.W. Peng-Jun Yao, Wen-Ling Chu, Yu-Wen Hao, Preparation and characterization of La_{12-x}Sr_xFeO₃ materials and their formaldehyde gas-sensing properties, *J. Mater. Sci.* 48 (2013) 441–450.
- [164] R. Hu, J. Wang, P. Chen, Y. Hao, C. Zhang, X. Li, Preparation of Cd-loaded In₂O₃ hollow nanofibers by electrospinning and improvement of formaldehyde sensing performance, *J. Nanomater.* 2014 (2014) 7.
- [165] Y.Q.H. Wang, H. Chen, Z. Lin, K. Dai, Highly selective n-butanol gas sensor based on mesoporous SnO₂ prepared with hydrothermal treatment, *Sens. Actuators B* 201 (2014) 153–159.
- [166] L. Deng, X. Ding, D. Zeng, S. Tian, H. Li, C. Xie, Visible-light activate mesoporous WO₃ sensors with enhanced formaldehyde-sensing property at room temperature, *Sens. Actuators B* 163 (2012) 260–266.
- [167] F. Qu, Y. Wang, J. Liu, S. Wen, Y. Chen, S. Ruan, Fe₃O₄–NiO core-shell composites: Hydrothermal synthesis and toluene sensing properties, *Mater. Lett.* 132 (2014) 167–170.
- [168] N.-H. Kim, S.-J. Choi, D.-J. Yang, J. Bae, J. Park, I.-D. Kim, Highly sensitive and selective hydrogen sulfide and toluene sensors using Pd functionalized WO₃ nanofibers for potential diagnosis of halitosis and lung cancer, *Sens. Actuators B* 193 (2014) 574–581.
- [169] V.S. Vaishnav, S.G. Patel, J.N. Panchal, Development of indium tin oxide thin film toluene sensor, *Sens. Actuators B* 210 (2015) 165–172.
- [170] H.-S. Woo, C.-H. Kwak, J.-H. Chung, J.-H. Lee, Highly selective and sensitive xylene sensors using Ni-doped branched ZnO nanowire networks, *Sens. Actuators B* 216 (2015) 358–366.
- [171] Y. Zeng, T. Zhang, L. Wang, M. Kang, H. Fan, R. Wang, Y. He, Enhanced toluene sensing characteristics of TiO₂-doped flowerlike ZnO nanostructures, *Sens. Actuators B* 140 (2009) 73–78.
- [172] S. Liu, Z. Wang, H. Zhao, T. Fei, T. Zhang, Ordered mesoporous Co₃O₄ for high-performance toluene sensing, *Sens. Actuators B* 197 (2014) 342–349.
- [173] X.S.C. Sun, F. Xiao, C. Niu, J. Wang, Synthesis of nearly monodisperse Co₃O₄ nanocubes via a microwave-assisted solvothermal process and their gas sensing properties, *Sens. Actuators B* 157 (2011) 681–685.
- [174] X.S.J. Park, G. Wang, Solvothermal synthesis and gas-sensing performance of Co₃O₄ hollow nanospheres, *Sens. Actuators B* 136 (2009) 494–498.
- [175] C.L.H. Shan, L. Liu, J. Zhang, H. Li, Z. Liu, X. Zhang, X. Bo, X. Chi, Excellent toluene sensing properties of SnO₂–Fe₂O₃ interconnected nanotubes, *ACS Appl. Mater. Interfaces* 5 (2013) 6376–6380.
- [176] Y.Z.L. Liu, G. Wang, S. Li, L. Wang, Y. Han, X. Jiang, A. Wei, High toluene sensing properties of Ni-O-SnO₂ composite nanofiber sensors operating at 330°C, *Sens. Actuators B: Chem.* 160 (2011) 448–454.
- [177] C.X.Z. Bai, S. Zhang, L. Zhang, Q. Zhang, W. Xu, J. Xu, Microstructure and gassensing properties of the ZnO thick film treated by hydrothermal method, *Sens. Actuators B* 151 (2010) 107–113.
- [178] M.Y.M.-H. Seo, T. Kida, J.-S. Huh, N. Yamazoe, K. Shimano, Microstructure control of TiO₂ nanotubular films for improved VOC sensing, *Sens. Actuators B* 154 (2011) 251–256.
- [179] F.M.H. Li, J. Liu, Y. Sun, Z. Jin, L. Kong, Y. Hu, J. Liu, Synthesis and gas sensing properties of hierarchical meso-macroporous SnO₂ for detection of indoor air pollutants, *Sens. Actuators B* 166 (2012) 519–525.
- [180] D. Han, P. Song, S. Zhang, H. Zhang, Q. Xu, Q. Wang, Enhanced methanol gas-sensing performance of Ce-doped In₂O₃ porous nanospheres prepared by hydrothermal method, *Sens. Actuators B* 216 (2015) 488–496.
- [181] P.D.P.C. Doroftei, F. Iacomi, Synthesis of nanocrystalline La-Pb-Fe-Operovskite and methanol-sensing characteristics, *Sens. Actuators B* 161 (2012) 977–981.
- [182] X.G.L.N. Chen, X.Y. Wang, J. Yu, J. Wang, Z.N. Tang, S.A. Akbar, Enhanced room temperature sensing of Co₃O₄-intercalated reduced graphene oxide based gas sensors, *Sens. Actuators B* 188 (2013) 902–908.
- [183] R.V.L. Yadava, R. Dwivedi, Sensing properties of CdS-doped tin oxide thick film gas sensor, *Sens. Actuators B* (2010) 37–42.
- [184] R.K.N.P.P. Sahay, Al-doped ZnO thin films as methanol sensors, *Sens. Actuators B* 134 (2008) 654–659.
- [185] K.R.M. Parmar, Copper (II) oxide thin film for methanol and ethanol sensing, *Int. J. Smart Sens. Intell. Syst.* 4 (2011) 710–725.
- [186] J. Qin, Z. Cui, X. Yang, S. Zhu, Z. Li, Y. Liang, Three-dimensionally ordered macroporous La_{1-x}Mg_xFeO₃ as high performance gas sensor to methanol, *J. Alloy. Compd.* 635 (2015) 194–202.
- [187] L. Sun, H. Qin, K. Wang, M. Zhao, J. Hu, Structure and electrical properties of nanocrystalline La_{1-x}Ba_xFeO₃ for gas sensing application, *Mater. Chem. Phys.* 125 (2011) 305–308.
- [188] C. Feng, S. Ruan, J. Li, B. Zou, J. Luo, W. Chen, W. Dong, F. Wu, Ethanol sensing properties of La_{Co_x}Fe_{1-x}O₃ nanoparticles: Effects of calcination temperature, Co-doping, and carbon nanotube-treatment, *Sens. Actuators B* 155 (2011) 232–238.
- [189] P. Song, H. Zhang, D. Han, J. Li, Z. Yang, Q. Wang, Preparation of biomorphic porous LaFeO₃ by sorghum straw biotemplate method and its acetone sensing properties, *Sens. Actuators B* 196 (2014) 140–146.
- [190] J. Guo, J. Zhang, D. Ju, H. Xu, B. Cao, Three-dimensional SnO₂ microstructures assembled by porous nanosheets and their superior performance for gas sensing, *Powder Technol.* 250 (2013) 40–45.
- [191] A. Teeramongkonrasmee, M. Sriyudthak, Methanol and ammonia sensing characteristics of sol-gel derived thin film gas sensor, *Sens. Actuators B: Chem.* 66 (2000) 256–259.
- [192] H.M. Yang, S.Y. Ma, G.J. Yang, W.X. Jin, T.T. Wang, X.H. Jiang, W.Q. Li, High sensitive and low concentration detection of methanol by a gas sensor based on one-step synthesis α-Fe₂O₃ hollow spheres, *Mater. Lett.* 169 (2016) 73–76.
- [193] L. Zhang, J. Zhao, J. Zheng, L. Li, Z. Zhu, Hydrothermal synthesis of hierarchical nanoparticle-decorated ZnO microdisks and the structure-enhanced acetylene sensing properties at high temperatures, *Sens. Actuators B* 158 (2011) 144–150.
- [194] N. Tamaekong, C. Liewhiran, A. Wisitsoraat, S. Phanichphant, Acetylene sensor based on Pt/ZnO thick films as prepared by flame spray pyrolysis, *Sens. Actuators B* 152 (2011) 155–161.
- [195] X. Wang, M. Zhao, F. Liu, J. Jia, X. Li, L. Cao, C₂H₂ gas sensor based on Ni-doped ZnO electrospun nanofibers, *Ceram. Int.* 39 (2013) 2883–2887.
- [196] T.Z. Qi Qi, Xuejun Zhengb, Huitao Fana, Li Liua, Rui Wang, Yi Zeng, Electrical response of Sm₂O₃-doped SnO₂ to C₂H₂ and effect of humidity interference, *Sens. Actuators B* 134 (2008) 36–42.
- [197] Z.I.C.L.F. Dong, Z.K. Zhang, Gas sensing properties of nano-ZnO prepared by arc plasma method, *Nanostruct. Mater.* 8 (1997) 815–823.
- [198] A.S.M. Iftekhar Uddin, K.-W. Lee, G.-S. Chung, Acetylene gas sensing properties of an Ag-loaded hierarchical ZnO nanostructure-decorated reduced graphene oxide hybrid, *Sens. Actuators B* 216 (2015) 33–40.
- [199] A.S.M. Iftekhar Uddin, D.-T. Phan, G.-S. Chung, Low temperature acetylene gas sensor based on Ag nanoparticles-loaded ZnO-reduced graphene oxide hybrid, *Sens. Actuators B* 207 (2015) 362–369.
- [200] A.S.M.I. Uddin, G.-S. Chung, Synthesis of highly dispersed ZnO nanoparticles on graphene surface and their acetylene sensing properties, *Sens. Actuators B* 205 (2014) 338–344.
- [201] M.-T. Ke, M.-T. Lee, C.-Y. Lee, L.-M. Fu, A MEMS-based benzene gas sensor with a self-heating WO₃ sensing layer, *Sensors* 9 (2009) 2895–2906.
- [202] L. Wang, R. Zhang, T. Zhou, Z. Lou, J. Deng, T. Zhang, Concave Cu₂O octahedral nanoparticles as an advanced sensing material for benzene (C₆H₆) and nitrogen dioxide (NO₂) detection, *Sens. Actuators B* 223 (2016) 311–317.
- [203] K.Y.J. Huang, C. Guo, M. Zhai, Y. Wu, M. Yang, J. Liu, Preparation of porous flower-shaped SnO₂ nanostructures and their gas-sensing property, *Sens. Actuators B* 147 (147) (2010) 467–474.
- [204] V.S. Vaishnav, S.G. Patel, J.N. Panchal, Development of ITO thin film sensor for detection of benzene, *Sens. Actuators B* 206 (2015) 381–388.
- [205] X. Gao, X. Su, C. Yang, F. Xiao, J. Wang, X. Cao, S. Wang, L. Zhang, Hydrothermal synthesis of WO₃ nanoplates as highly sensitive cyclohexene sensor and high-efficiency MB photocatalyst, *Sens. Actuators B* 181 (2013) 537–543.
- [206] X. Gao, C. Yang, F. Xiao, Y. Zhu, J. Wang, X. Su, WO₃·0.33H₂O nanoplates: hydrothermal synthesis, photocatalytic and gas-sensing properties, *Mater. Lett.* 84 (2012) 151–153.
- [207] M.Y.J. Huang, C. Gu, M. Zhai, Y. Sun, J. Liu, Hematite solid and hollow spinels: Selective synthesis and application in gas sensor and photocatalysis, *Mater. Res. Bull.* 46 (2011) 1211–1221.
- [208] B.T.C. Raut, M.A. Nalage, S.R. Dalavi, D.S. Mali, Sawanta Patil, P.S. Patil, V. B., CSA doped polyaniline/CdS organic-inorganic nanohybrid: physical and gas sensing properties, *Ceram. Int.* 38 (2012) 5501–5506.
- [209] H. Gong, Y.J. Wang, S.C. Teo, L. Huang, Interaction between thin-film tin oxide gas sensor and five organic vapors, *Sens. Actuators B* 54 (1999) 232–235.
- [210] G. Korotcenkov, B.K. Cho, Engineering approaches for the improvement of conductometric gas sensor parameters: Part 1. Improvement of sensor sensitivity and selectivity (short survey), *Sens. Actuators B: Chem.* 188 (2013) 709–728.
- [211] X. Li, J. Liu, H. Guo, X. Zhou, C. Wang, P. Sun, X. Hu, G. Lu, Au@In₂O₃ core-shell composites: a metal-semiconductor heterostructure for gas sensing applications, *RSC Adv.* 5 (2015) 545–551.
- [212] G. Konvalina, H. Haick, Effect of humidity on nanoparticle-based chemiresistors: a comparison between synthetic and real-world samples, *ACS Appl. Mater. Interfaces* 4 (2011) 317–325.
- [213] B. de Lacy Costello, R.J. Ewen, N.M. Ratcliffe, P. Sivanand, Thick film organic vapour sensors based on binary mixtures of metal oxides, *Sens. Actuators B* 92 (2003) 159–166.